A STUDY OF THE NIGHTTIME GROWTH OF SECONDARY ORGANIC AEROSOL USING THE CAPTIVE AEROSOL GROWTH AND EVOLUTION INSTRUMENT SUITE

A Thesis

by

JILLIANNE RENE MATUS

Submitted to the Office of Graduate and Professional Studies of
Texas A&M University
in partial fulfillment of the requirements for the degree of

MASTER OF SCIENCE

Chair of Committee,	Don Collins
Committee Members,	Sarah D. Brooks
	Shari Yvon-Lewis
Head of Department,	Ping Yang

December 2017

Major Subject: Atmospheric Sciences

ABSTRACT

Models that seek to calculate the effect of aerosol on climate must take into account both primary and secondary sources of aerosol, as well as the environmental conditions that may affect these populations such as ambient temperature, RH, UV intensity, and gas composition. These factors can prompt changes in the physical and chemical properties of the aerosols, affecting the way they contribute to climate change and interact with other atmospheric constituents. Recently, there has been particular interest in the aerosol that is formed from the combination of urban and rural air masses. Studies have shown that the interaction between biogenic volatile organic compounds (BVOC) and anthropogenic emissions is likely a major source of secondary organic aerosol (SOA). The unique ability to isolate factors contributing to SOA formation processes within the complex ambient environment allows the CAGE system to provide insight into anthropogenic impacts and guide related modeling and mitigation efforts. This research project aims to demonstrate the suitability of the new CAGE system for observing trends in particle growth rate. Experiments were performed in the W G Jones State Forest in the greater Houston metropolitan area, which provided a favorable location for observing aerosol production resulting from different concentrations of ambient gases. Particular focus will be on the growth and stability of particles formed during nighttime observations. It would be expected that SOA would lose mass as the concentration of gases that contribute to their formation decreases. However, multiple days of observation showed that this was not often the case, indicating that the aerosol

formed was relatively stable and unaffected by perturbations in the concentration of atmospheric constituents.

ACKNOWLEDGEMENTS

I would like to thank Dr. Collins for inviting me into his research group and for his patience and guidance throughout this project. My mentors Dr. Shanna Ratnesar-Shumate and Dr. Paul Dabisch have been a source of constant encouragement; I will always be grateful to them for having confidence in me and for the opportunities for growth and development that they have provided me. Much thanks goes to Gabriel Antonietti for first putting a drill in my hands and teaching me to just jump in and tackle problems that may seem daunting at first. Thanks also to Chance Spencer and countless undergraduate and graduate students, for all of the hard work that went into building these chambers and their predecessors. Most of all I'd like to thank my husband, Nathan, for his love, support and patience.

CONTRIBUTORS AND FUNDING SOURCES

Contributors

This work was supported by a thesis committee consisting of Professor Don Collins and Professor Sarah Brooks of the Department of Atmospheric Science and Professor Shari Yvon-Lewis of the Department of Oceanography.

Many graduate and undergraduate students worked on this test system and its predecessors, including but not limited to: Nathan Taylor, Chance Spencer, Gabriel Antonietti, Manuel Salgado, Behdad Yazdani, Calvin Owens, and Jianfei Peng.

Funding Sources

Graduate study was supported by a fellowship from Texas A&M University and by research grants from the National Science Foundation and the Defense Threat Reduction Agency.

TABLE OF CONTENTS

Page

LIST OF FIGURES

Page

LIST OF TABLES

Page

CHAPTER I

INTRODUCTION AND LITERATURE REVIEW

The significant impact of atmospheric aerosols on human health and climate change warrants extensive research into their various sources and formation mechanisms. The World Health Organization estimates that 7 million premature deaths in 2012 could be attributed to air pollution. Studies have shown that particles with a diameter less than 2.5 μm (PM2.5) are especially damaging to human health. These particles are small enough to penetrate deep into the lung, causing irritation to the lining of the airways and potentially translocating into the bloodstream (Harrison and Yin, 2000; Bennett, 2002). Epidemiological evidence has shown a link between PM2.5 exposure and cardiovascular disease and mortality (Atkinson *et al*., 2010; Atkinson *et al.*, 2014). The impact of aerosols on the environment is also a source of great uncertainty in climate models (IPCC 2013). Environmental conditions such as UV intensity and ambient gas composition can cause changes in the chemical composition of a given aerosol population over time (Grosjean and Seinfeld, 1989). This can result in alterations to the physical and chemical properties of the aerosol, affecting the way it contributes to climate change and its interaction with other atmospheric constituents. Studies that seek to understand the formation mechanisms and processing of aerosols under various atmospheric conditions are an important step towards predicting and potentially mitigating the negative effects of aerosol on human health and climate.

1.1 SOA Formation Mechanisms

There are many aerosol sources, which are generally sorted into a four-category matrix with pairs of: anthropogenic or natural, and primary or secondary. Anthropogenic aerosol includes that produced from man-made processes, and includes aerosol types such as soot and primary organic aerosol (POA) from incomplete combustion of fossil fuels. While this does account for a significant portion of the aerosol mass in an urban environment, the vast majority on average is non-anthropogenic in origin, and includes sources such as sea salt, dust, and particulates emitted by volcanoes (IPCC 2013). Studies have shown that more than half of submicron atmospheric aerosol mass has a significant organic component (Zhang *et al*. 2007, Jimenez *et al*., 2009). This organic component has diverse sources including primary emissions from fossil fuel combustion and biomass burning, and secondary aerosol formation, which is believed to be largely driven by biogenic gas emissions. A recent study that was conducted at both a rural and an urban site in the southeastern United States showed that up to 76% of submicron aerosol was composed of organic material across multiple seasons (Budisulistiorini *et al*. 2016). This submicron aerosol undergoes processing in the atmosphere to form a large portion of the calculated atmospheric aerosol budget that is not well accounted for – secondary organic aerosol (SOA).

Studies have shown that the interaction between biogenic volatile organic compounds (BVOC) and anthropogenic emissions of aerosols and trace gases is likely a major source of SOA (Pandis *et al*. 1993, de Gouw *et al*. 2008). SOA is formed when organic gaseous constituents in the atmosphere undergo oxidative reactions that make

them less volatile and therefore more prone to gas-to-particle conversion through condensation onto existing particles. Biogenic hydrocarbons, such as monoterpenes and isoprene, are prevalent in the atmosphere across much of the globe and are believed to be significant contributors to the SOA budget due to their high reactivity with atmospheric oxidants such as ozone, O_3, hydroxyl radical, OH, and nitrate radical, NO_3. The emission rates of these BVOCs are largely dependent on temperature and/or the intensity of solar radiation (Fuentes *et al*., 2000). Deciphering the formation mechanisms of SOA could serve an important role in developing more accurate climate models, and could be a contributing factor in affecting environmental regulation of SOA precursors that may or may not currently be considered environmental pollutants. Without a more accurate assessment of the formation mechanisms of these oxidation byproducts, climate models are missing an important piece of the radiative forcing equation.

Oxidation can occur through multiple pathways, the relative importance of which varies with several factors including the concentration of oxidative compounds such as OH, O_3 or NO_3 and their associated rate constants. NO_3 has a high rate constant with many SOA precursors, but because it is highly photoreactive and reactive with NO, it is primarily present at concentrations high enough to significantly contribute to SOA formation at night. Hydroxyl radical is the most prevalent oxidant in the troposphere, with many formation pathways. A compound's reaction rate with OH will often determine its lifetime in the atmosphere. Ozone naturally exists in the troposphere at low concentrations. Photooxidation of hydrocarbons and NO emitted from, among other sources, fossil fuel combustion can lead to high concentrations of ozone that have been

shown to negatively affect human health and provide an oxidation pathway for SOA precursors. NO_x has a significant influence on the production of all the aforementioned oxidative compounds in urban environments, which makes it an important component of the SOA formation mechanism. NOx is emitted during combustion both from reaction of nitrogen present in the fuel and from reaction of N_2 and O_2 at high temperature.

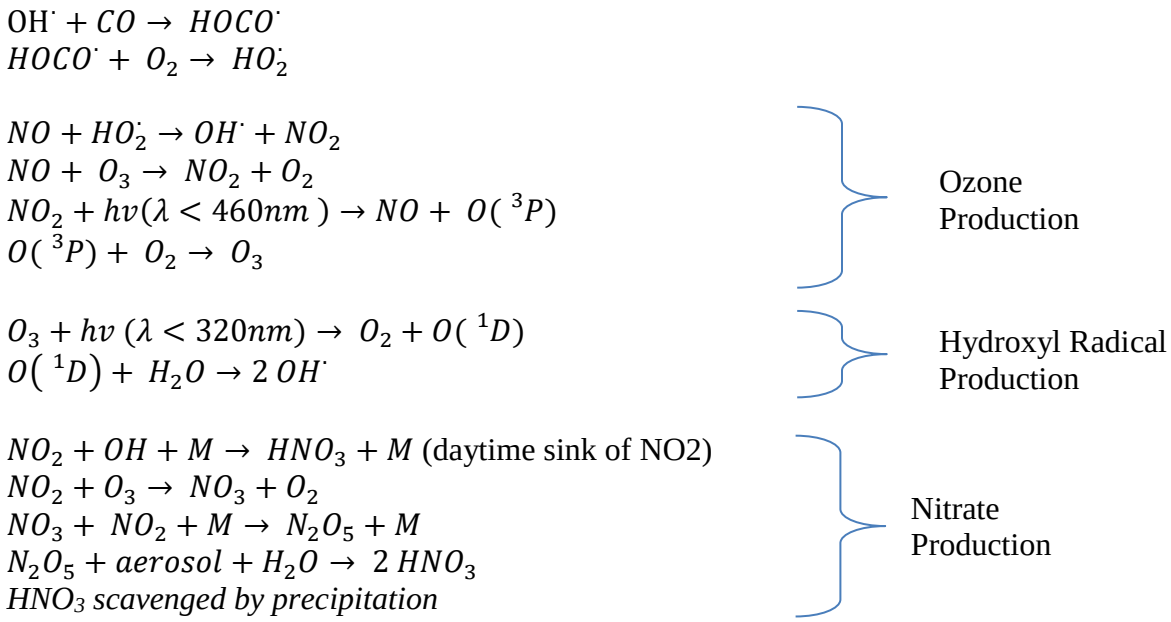

Figure 1: Reactions contributing to the production of O_3, OH, and NO_3

Hydroxyl radical concentration tends to decrease as nighttime progresses as its main sources are tied to photochemistry and its high reactivity results in a short atmospheric lifetime. Because of this and the cessation of its photolysis at night, NO_3 radical has the potential to be the predominant nighttime oxidant leading to SOA growth. Yields of NO_3 radical-driven aerosol formation will depend largely on the types of biogenic precursor gases available. Chamber experiments with NO_3 radical and isoprene

under no-UV conditions led to high yields of organic nitrates, which undergo further oxidative processing to form condensable products that could contribute to SOA production (Ng *et al*., 2007, and Rollins *et al*., 2009). However, the oxidation byproducts of the NO_3-isoprene reaction are typically fairly volatile, so they are not considered a strong source of isoprene derived SOA. Models have estimated the fraction of isoprene oxidized by NO_3 radical to account for only 6-7% of the total globally (Ng *et al.*, 2007). Other biogenic gases, particularly monoterpenes, have shown a strong correlation with nitrate radical driven SOA growth in several recent studies. As part of a field study conducted in the southeastern U.S., Xu *et al*. (2015) concluded that the reaction of nitrate radical and monoterpenes accounts for 50% of the nighttime organic aerosol production. A field study by Rollins *et al*. (2012) showed that the SOA containing oxidation byproducts of nitrate increased from 2.3% of the total organic aerosol at sunset to 4.7% at 11:30 PM. Since the concentrations of oxidants other than nitrate radical are typically lower at night, nighttime particle growth mechanisms have the potential to be more easily analyzed due to the reduction in competing reaction mechanisms.

1.2 SOA Reversibility

Estimates of the global production of SOA vary greatly among researchers. Griffin *et al*. (1999) estimated 13-24 Tg/yr are formed, Chung and Seinfeld (2002) put the yearly production at 11.2 Tg, and calculations by Derwent *et al*. (2003) result in a total of 63 Tg/yr. Global SOA contributions from isoprene oxidation alone have been estimated to be as high as 6.2 Tg/yr (Henze and Seinfeld 2006). Further complicating

these calculations, many of the current climate models treat SOA formation as a reversible process (Tsigaridis and Kanikidou, 2003) – particles grown through the condensation of low volatility vapors can decrease in size when their surrounding environment is perturbed, by either a decrease in the concentration of relevant gases, an increase in temperature, or a decrease in relative humidity. At its simplest form, the tendency for particles to increase or decrease in size due to the evaporation or condensation of semi-volatile components can be described by the following equations from Seinfeld and Pandis (2016).

$$\frac{\partial n(v,t)}{\partial t} = -\frac{\partial}{\partial v}[I_v(v,t)n(v,t)] \qquad \text{(Equation 1)}$$

$$I_{(v)} = \frac{2\pi^{2/3}(6v)^{1/3}D_i M_i}{\rho_p RT} f(Kn, \propto)(p_i - p_{eq,i}) \qquad \text{(Equation 2)}$$

Where: $v = \frac{1}{6}\pi D_p^{\ 3}$

D_i = diffusion coefficient for species *i* in air

M_i = molecular weight of species *i*

f(Kn,α) = the correction due to noncontinuum effects and imperfect surface accommodation

$p_i - p_{\mathrm{eq},i}$ = the difference in the vapor pressure of *i* far from the particle and the equilibrium vapor pressure

After gas-to-particle conversion, reactions may take place inside or on the surface of the particle that render the recently condensed compounds less volatile, with

the result that changes to the environment are less likely to cause the evaporation of the condensed products.

Chamber experiments aimed at measuring the cause and extent of SOA evaporation and the resulting particle shrinkage due to either dilution or heating have shown that less shrinkage occurs than would be expected for an aerosol population whose condensed products are in equilibrium with their gas phase species. In experiments with the monoterpene limonene and its NO_3 radical derived SOA, Boyd *et al.* (2017) found that little evaporation occurred due to either dilution or heating (at atmospherically relevant temperatures), indicating that the products formed were only semi-volatile. Grieshop *et al*. (2007) found that the rate of evaporation of SOA formed from the ozonolysis of α-pinene was much lower than that of single component aerosol of a similar size when diluted. It should be noted that these experiments were performed at unnaturally high gas and particle concentrations, and since concentration may affect the composition of the SOA formed, the observed effects may not be representative of SOA reversibility occurring in nature. However, SOA evaporation is believed to be responsible for apparent particle shrinkage observed in field measurements, and is often associated with atmospheric dilution events or high temperature and low relative humidity (Young *et al*., 2012; Skrabalova *et al.*, 2015; Cusack *et al*., 2013). It is difficult to attribute shrinkage to SOA formed from a particular chemical reaction in field experiments without detailed chemical analysis of both the aerosol and the ambient gases due to the multitude of potential contributing factors. Further studies, both in the laboratory and the field, are needed for more accurate modelling of SOA reversibility.

1.3. SOA Study Methods

There are two ways in which SOA formation is typically studied –through field measurements and controlled chamber systems. Aerosol chamber experiments are often used to isolate the various reaction mechanisms that lead to SOA formation. Most aerosol chambers are suspended in large rooms that are lined with blacklights to allow for photochemical experiments. For example, Caltech has a pair of 28 m^3 FEP Teflon lined chambers with ports for the injection of controlled concentrations of gases and seed particles. Several laboratories utilize large Teflon bags suspended in rooms that have temperature control and air purification systems (e.g., University of California Riverside, Carnegie Mellon University). One of the major limitations of these systems is that the duration of the experiments that can be conducted is dictated by the loss rate of the particles under study. Stirred settling or rotating drums have been used for aerosol aging experiments to increase particle residence time, though these systems require more sophisticated engineering controls to reduce particle losses due to turbulent mixing and to allow for sampling during chamber rotation.

Chamber experiments are typically performed in batches – the initial experiment conditions are prescribed and then the system is closed and the results of the reactions are either measured periodically throughout the experiment or at the conclusion. This controlled environment approach does not provide an accurate representation of the multitude of changing conditions that an aerosol population is subject to and affected by. However, the importance of understanding the effect of individual factors on particle growth cannot be discounted. While the results may not always be directly applicable to

the real-world environment, oftentimes field studies have too many variables to enable definite conclusions and chamber studies can provide the best avenue for piecing together the contributing factors.

1.4. Research Objectives

This research project focuses on the development of a system for studying the aging of a controlled aerosol population with exposure to various atmospheric conditions as well as the results of experiments performed with this system. The Captive Aerosol Growth and Evolution (CAGE) instrument suite uses new and tested design features to bridge some of the gaps in existing chamber research. As a field-deployable system, the CAGE chambers are capable of performing in situ ambient air experiments under the influence of photochemistry with various controlled chemical and environmental perturbations. This instrumentation suite bridges the gap between field and chamber experiments. Experiments were performed in the W G Jones State Forest in the greater Houston metropolitan area, which provided an ideal location for looking at the effects of varying concentrations of BVOCs and anthropogenic gases on the growth of generated seed particles. The results presented will focus on the nighttime growth of aerosol and the reversibility of this growth as the concentration of relevant gases that can contribute to gas-to-particle condensation decreases.

CHAPTER II

DESIGN OF A CONTROLLED ENVIRONMENT CAPTIVE AEROSOL CHAMBER SYSTEM

The CAGE chambers use new and tested design features to bridge some of the gaps in existing chamber research. The CAGE system has the potential to uniquely inform our understanding of SOA formation mechanisms, respective anthropogenic influences, and reversibility. Such understanding will aid in accurate modeling of SOA formation processes, which in turn will allow modeling of the effects of SOA on climate, visibility, and human health. This chapter presents the unique design specifications and capabilities of the CAGE chamber system relevant to the data obtained for this thesis.

The CAGE chamber system is composed of two identical chambers to enable experiments with one chamber acting as the test chamber and one acting as the control. Two single sheets of heat-sealed Teflon FEP (fluorinated ethylene polypropylene) make up the walls of each chamber. FEP was chosen for its high UV transmittance and because it is unlikely to off-gas and affect particle growth rates. In a typical experiment set-up, one chamber is provided with a carbon- and aerosol-scrubbed circulated gas volume and the other with aerosol-scrubbed ambient air. Shrouds are used to cover one or both chambers for experiments under dark conditions.

Control of the gas phase is accomplished by capping one end of the reactor volume with an expanded polytetrafluoroethylene (ePTFE) membrane and rapidly circulating air through the surrounding enclosure. PTFE is a carbon-fluorine polymer

that is extremely nonpolar and nonreactive and the fibrous expanded variant (ePTFE) is designed to act as a barrier to particles while allowing gases to pass through at a high flow rate (Figure 2) (Wikol *et al*., 2007). A blower is used to pull air out of the enclosure so that fresh ambient air is constantly circulated through the system. A PTFE mesh sheet stretched across the inlet of the enclosure on the roof helps to scrub insects and large particles from the air entering the enclosure. Activated carbon is placed in the inlet when experiments with low organic gas concentrations are desired. Without the carbon in place, the chambers can track ambient gas composition. Predecessors of the CAGE system have proven the efficiency of ePTFE at allowing a controlled volume to track the concentration of ambient gases while retaining a constant aerosol population. As an example, Figure 3 shows the relationship between the mixing ratio of ozone alternately measured inside and just outside of a similar chamber (the data shown is from experiments performed by a former Texas A&M Atmospheric Sciences graduate student).

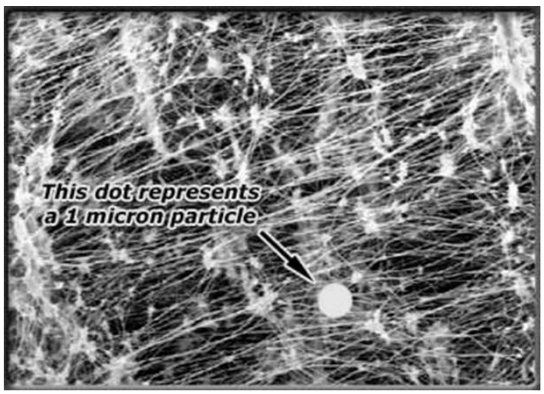

Figure 2: SEM image of ePTFE membrane with 1 μm dot for reference

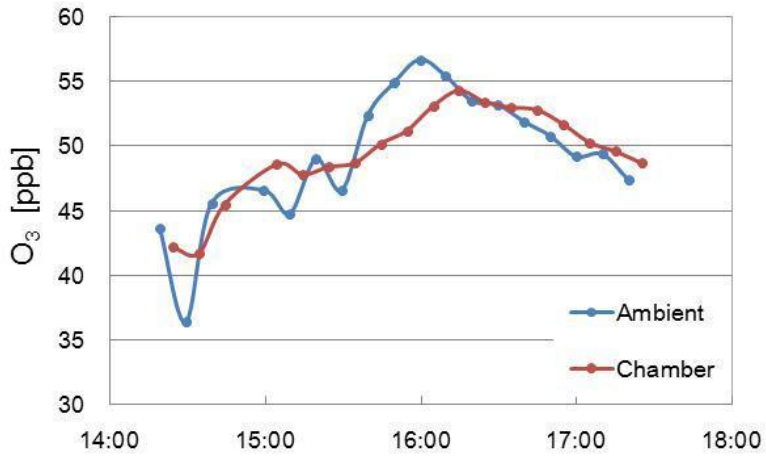

Figure 3: Comparison of ambient vs. chamber O_3 mixing ratio in the CAGE predecessor AACES chamber (Peng, 2010)

Particle lifetime in the system is enhanced through the use of drive shaft motors that rotate both chambers at about 1 rpm. This slow rotation is a method commonly used in the bioaerosol community to increase particle retention time. As the particles settle due to gravity, their direction is constantly changing due to the rotation of the volume of air they are entrained in. This causes the particles to move in a spiral pattern, which is governed by the radius of their orbit and the centrifugal acceleration imparted by the rotation of the drum, as described by Equations 3 and 4, respectively (Goldberg, 1958).

$$r_0 = \frac{d_p^2 \cdot g \cdot \rho \cdot C_c}{18 \cdot \mu \cdot \omega} \quad \text{(Equation 3)}$$

$$V(r) = \frac{m \cdot \omega^2 \cdot r \cdot C_c}{3 \cdot \pi \cdot \mu \cdot d_p} \quad \text{(Equation 4)}$$

Where: r_0 = particle orbit radius
g = gravitational constant
ρ = particle density
C_c = slip correction factor
μ = dynamic viscosity of the air
ω = drum rotation rate
V(r) = outward particle velocity at radial position r

The rotation must be smooth and uniform to reduce any potential sources of mixing that would decrease the particle residence time in the system through wall losses induced by turbulent and Brownian diffusion. Losses due to electrostatic drift are also a concern, especially because of the high electrostatic potential of the Teflon material used for the chamber wall. Polonium-210 strips placed on the platform beneath the chambers provides a source of bipolar ions to the ambient air that help to dissipate static charge on the chamber walls.

Acrylic with enhanced UV transparency was used for the walls of the enclosure to allow for the transmission of the maximum amount of solar radiation. Opaque panels were used to cover the walls of the enclosure before experiments were begun to prevent photochemical reactions from taking place before the generated aerosol population was injected and measured. To reduce the likelihood of contamination from machining oil and various other potential sources in the frame of the chambers, all surfaces were wrapped in PTFE tape that had been baked in an industrial oven to evaporate any VOCs

that may remain from the manufacturing process. Rotation of the chambers was enabled via a chain-drive motor that turned a sprocket attached to the central shaft of the chamber. This shaft also served as the port for both the aerosol injection and sampling lines.

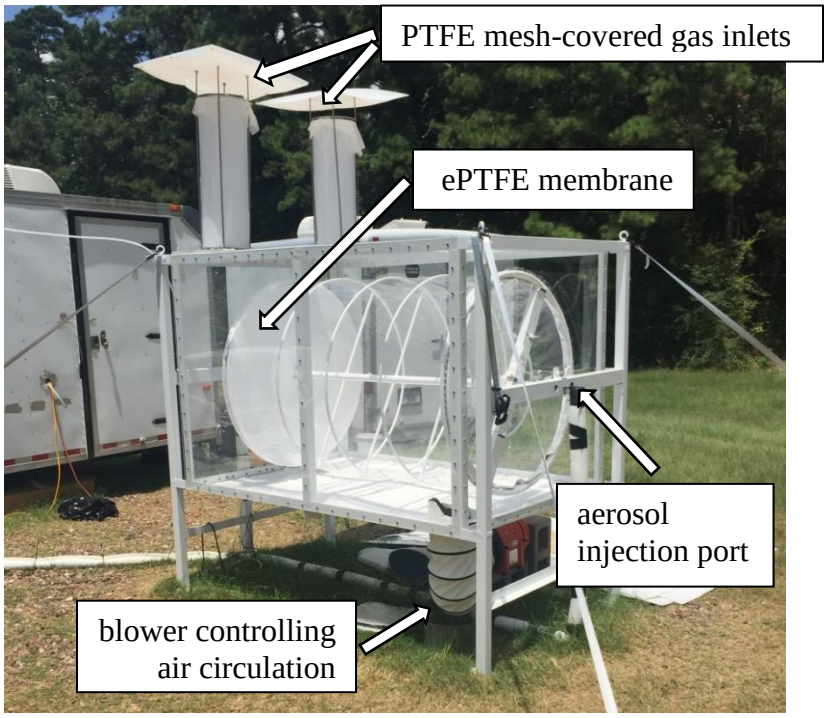

Figure 4: Single chamber with solar shield removed

Figure 5: Both chambers with solar shields in place

Seed aerosols were injected via an angled inlet to help ensure mixing within the chamber for a more homogeneous aerosol population. Aerosol generation and size selection were performed with a separate system located in the instrument control trailer. A solution of ammonium sulfate was nebulized using a TSI 3076 aerosol generator. The aerosol was then passed through a desiccant dryer and a Po-210 charge neutralizer before entering the differential mobility analyzer (DMA) column. The DMA size selected the aerosol population so that monodisperse aerosol of a chosen electromobility diameter was injected into the chambers. The DMA was operated as a scanning mobility particle sizer (SMPS) for the periodic measurement of the size shift in the aerosol distribution throughout the course of an experiment.

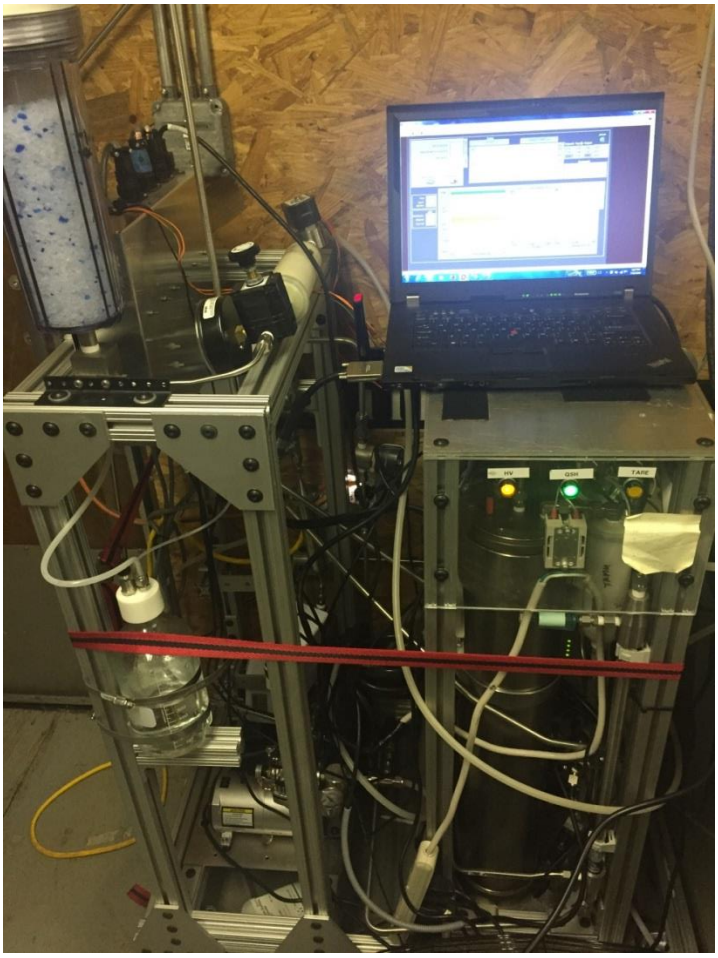

Figure 6: Photo of the aerosol generation system with the TSI aerosol generator 3076, desiccant dryer, and SMPS column

Valve control to enable injection or sampling of particles from the system was achieved with code written with National Instruments LabVIEW software. National Instruments Data Acquisition cards (NIDAQ) allow for the regulation of analog output and digital output signals with the accompanying software platform that enables the user to send voltages to connected devices. The NIDAQ cards also read analog input signals

from the SMPS so that data can be logged and analyzed. All processes, with the exception of removing or replacing the sun covers from the chambers, could be performed remotely through the use of the LabVIEW control software.

Aerosol samples were drawn approximately once per hour to monitor size changes in the captive population. Ambient gas measurements were taken concurrently at the site by Dr. James Flynn's group from University of Houston using an Ionicon quadrupole Proton Transfer Reaction – Mass Spectrometer (PTR-MS) and several Thermo Environmental trace gas analyzers. The W G Jones State Forest, located between Conroe and Spring in the northern suburbs of Houston (Figure 7), was chosen for the sampling location because it provided many potential sources of BVOC from the varied vegetation in the park, and because it is subject to significant concentrations of anthropogenic VOCs and oxidants due to its close proximity to the Houston area. Air mass source regions and trajectories for days of interest were tracked using the NOAA Hysplit model.

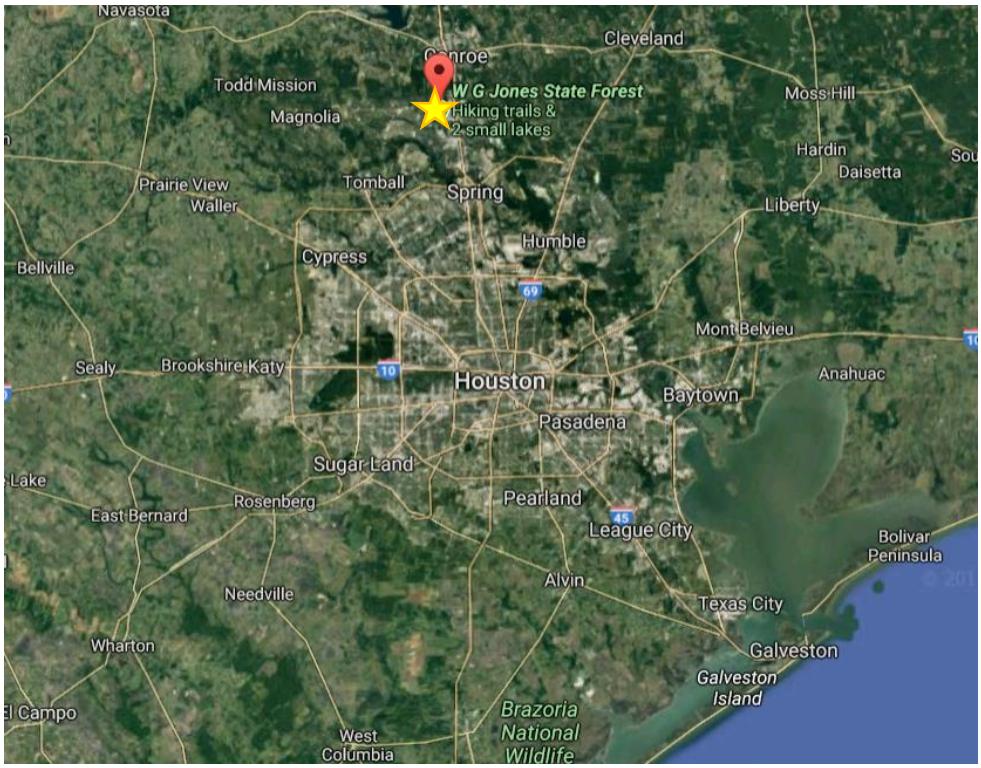

Figure 7: Map of the W G Jones State Forest in relation to the greater Houston metropolitan area

CHAPTER III

EXPERIMENTAL METHODS

Typical experiments involved the generation and injection into the chambers of two monodisperse seed aerosol populations. One population, which was around 300 nm diameter, was used to maintain a particle surface area concentration comparable to that outside. The second population, initially around 70 nm, was the population that was tracked throughout the experiment for calculating growth rate. The DMA size selected the aerosol and each population was first injected into one chamber, then the other. Once the desired concentrations had been reached, the generation would be stopped and measurements of the aerosol size distribution would be taken incrementally for approximately 5 minutes from each chamber.

Raw size distribution data were processed so that the injected modes could more easily be tracked. Over time the size distribution of the injected aerosol population would become less pronounced as aerosol escaped through small leaks in the chamber or was lost through deposition to the walls. Separating out the relevant modes from the background allowed for the calculation of growth rates. The data output of the SMPS is given in number concentration (or more precisely $dN/d\log D_p$) of particles in each size bin (of which there are 60, ranging from 20 nm to 487 nm diameter). A LabVIEW VI takes the raw distribution data and fits them to a lognormal distribution using an operator-input approximate peak particle diameter ($\overline{D}_p$) and standard deviation (σ) for the first distribution in a measurement series after excluding the tails of the distribution

and subtracting off a predetermined background distribution. The calculated $\overline{D}_p$ and σ of the initial distribution are then used as the starting point by the program to fit the subsequent distributions. The lognormal fit calculations are performed based on the following equation from Seinfeld and Pandis (2016) for ambient aerosol size distributions.

$$n^{\circ}{}_N(\log D_p) = \frac{N}{(2\pi)^{1/2}\log\sigma}\exp\left(-\frac{(\log D_p - \log \overline{D}_p)^2}{2\,log^2\sigma}\right) \qquad \text{(Equation 5)}$$

Where: $n^{\circ}{}_N(\log D_p)$ = the lognormally fitted number concentration for a given bin
N = the number concentration
σ = the standard deviation of the distribution
D_p = the aerosol size bin
$\overline{D}_p$ = the mean particle diameter

For each size bin of the SMPS, a new number concentration is calculated that uses an estimated mean particle diameter, standard deviation and number concentration for the total distribution. These new data points are then compared to the raw data by the mean squares error method. The VI then performs iterative calculations that change the $\overline{D}_p$, σ, and *N* values until a minimum mean square error value is reached.

An example of raw, unprocessed distributions is shown in Figure 8. The gradual increase in the location of the size distribution of the smaller, initially 70 nm, peaks can be observed, as well as the marked decrease in aerosol concentration resulting in less pronounced peaks.

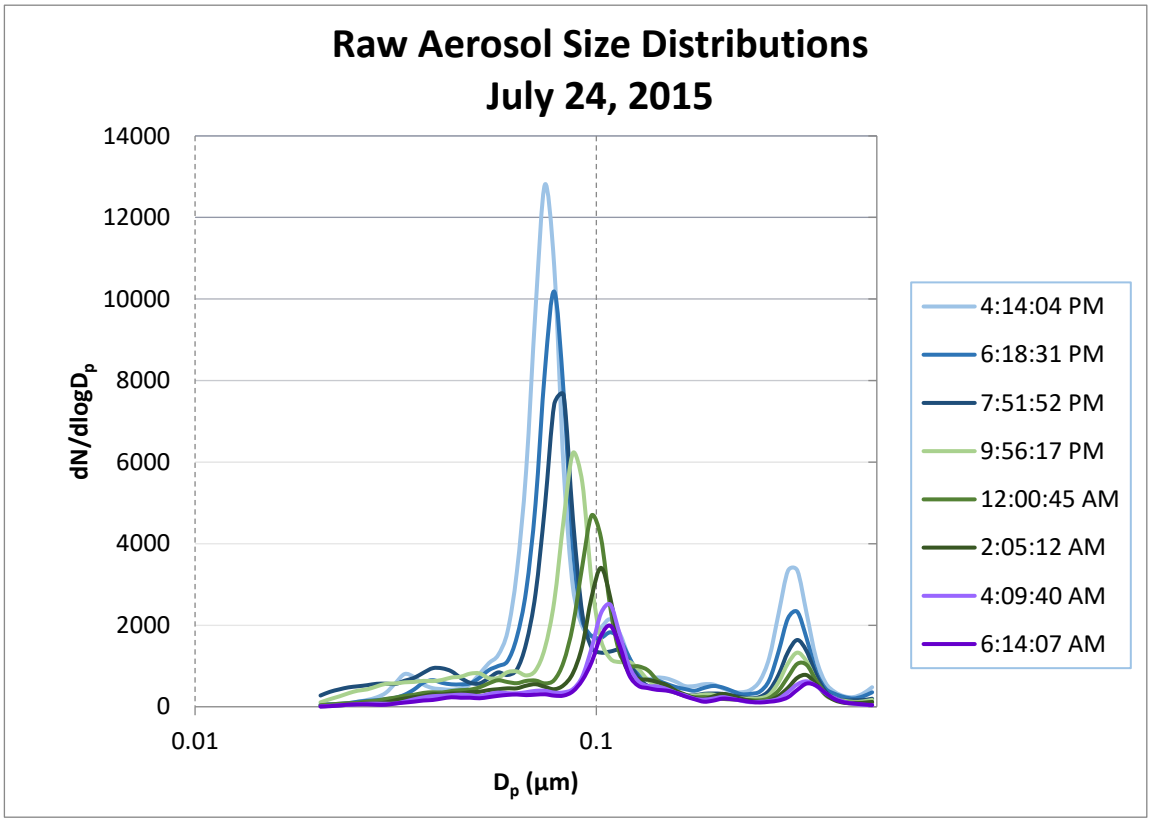

Figure 8: Example of raw size distribution data obtained with the SMPS

To quantify the change in particle size at each sampling timepoint, sequential SMPS size distributions were used to calculate growth rate (GR), which is simply the difference between the calculated fit diameter of the most recent sample ($d_{p,2}$) and the fit diameter of the previous sample ($d_{p,1}$) divided by the time difference between the two measurements (Equation 3). This provides a measure of the amount of mass that is gained or lost by the particle distribution as environmental conditions change.

$$GR = \frac{d_{p,2} - d_{p,1}}{t_2 - t_1} \qquad \text{(Equation 6)}$$

The PTR-MS measured the concentration of many VOCs in the ambient air, separated by their mass-to-charge (m/z) ratios. The m/z ratios for the measurements are then linked with those of known gases, though it is important to note that many gases have the same or indistinguishable m/z ratios so this does not always provide an accurate quantification of relevant gas concentrations. Particular focus was given to concentrations of monoterpenes and isoprene because they were typically the most concentrated of the VOCs that are known to contribute to SOA.

Assuming a steady-state approximation, and excluding sinks of NO_3 other than the reaction with NO, a rough estimate of the nighttime NO_3 concentration can be reached via the following expressions.

$$NO_2 + O_3 \rightarrow NO_3 + O_2 \qquad [1]$$

$$NO_3 + NO \rightarrow 2NO_2 \qquad [2]$$

$$[NO_3] \approx \frac{k_1 \cdot [NO_2] \cdot [O_3]}{k_2 \cdot [NO]} \qquad \text{(Equation 7)}$$

Where: k_1(298K) = 3.2 x 10^{-17} molec.$^{-1}$cm^{3}s^{-1} (Sander *et al.*, 2003)

k_2(298K) = 2.6 x 10^{-11} molec.$^{-1}$cm^{3}s^{-1} (Sander *et al.*, 2003)

This does not take into account the removal of NO_3 through conversion to HNO_3 or reactions with VOCs and can thus be considered a concentration upper bound. Equation 7 was used to calculate the approximate concentration of NO_3 based on measured NO_2, O_3 and NO concentrations. The NO_3 concentration was only calculated for measurements taken after sunset since Equation 7 does not include NO_3 removal through photolysis.

CHAPTER IV

RESULTS AND DISCUSSION

Particle growth rates on almost all of the nights during the study remained positive through most of the night, with only minor apparent response to decreases in the concentration of oxidant and/or oxidizable gases. A slight negative growth rate was often observed in the pre-dawn time period, indicating that the condensed species that contributed to particle growth earlier in the evening had evaporated to a minor extent. Previous studies have linked particle shrinkage to atmospheric dilution, high temperatures and low relative humidities (Young *et al*., 2013; Cusack *et al*., 2013). Of the 23 days on which measurements spanned the hours around sunset, only on 4 was the growth rate negative within 1 hour of sunset (either one hour before or one hour after). This is contrary to what might be expected considering that the concentrations of ozone and hydroxyl radical, two important oxidants, are typically decreasing at this time. This could be partially due to the decrease in temperature after sunset, which would help drive condensation of existing semi-volatile gases and could help explain why the particle growth rate continues to stay positive and in most cases increases in magnitude until a peak is typically reached between the hours of 9PM and 12AM. This could also be due to the nighttime increase in mixing ratio of another important oxidant, nitrate radical. Another consideration is that changes in the boundary layer around sunset can contribute to increased aerosol mass and gas concentrations due to reduced vertical mixing. Typically, the concentration of isoprene decreased at nightfall as the

photosensitive emissions stopped, while the concentration of monoterpenes often increased through the night.

Measured data were analyzed to look for patterns in the oxidant and oxidizable gas concentrations that might indicate what conditions are more favorable for forming oxidation products that have low volatility and are therefore less prone to re-volatilization. Temperature, RH and precipitation data at sunset were tracked for each day (Table 1). Table 2 summarizes the concentrations of relevant gases at both the time of the peak growth rate and at sunset for all days when a discernable peak in growth rate after sunset was observed. All days on which particle shrinkage occurred exhibited both high temperature and low RH around sunset, with the exception of July 30th, which had a relatively high RH and low temperature of 88% and 26°C. However, the extent of particle shrinkage on the 30th was less (-0.87 nm/hr) than on the other days and only lasted for one sample (meaning one of the hourly averaged 5 min collection periods), which could be attributed to noise in the data. There are several days on which high temperatures and low RH do not coincide with a particle shrinkage event, indicating that these factors are not the sole predictors of particle stability and suggesting that the aerosol population is at times comprised of components that are not prone to volatilization.

	Temp (°C)	RH (%)	Wind Speed (m/s)	Wind Direction
24-Jul	31.7	61	3.6	SE
27-Jul	31.7	57	4.1	SE
28-Jul	32.8	48	3.1	SE
29-Jul	33.3	45	2.1	SE
30-Jul	26.1	88	ND	ND
31-Jul	31.7	38	1.6	ENE
2-Aug	31.7	39	1.6	ESE
3-Aug	31.1	48	ND	ND
4-Aug	31.1	57	4.6	SSE
9-Aug	33.3	44	2.1	ESE
10-Aug	34.4	43	1.6	SE
24-Aug	30	70	ND	ND
27-Aug	26.7	67	ND	ND

Table 1: Meteorological conditions measured between 7:50 and 8 PM. Days on which a negative growth rate was observed between the hours of 7 PM and 9 PM are highlighted in yellow (www.wunderground.com)

Gases measured by the PTR-MS include methanol, acetaldehyde, acetone, isoprene, methyl vinyl ketone (MVK)/pentene, methyl ethyl ketone (MEK)/butanal, benzene, toluene, the xylenes, trimethylborane (TMB), and the monoterpenes. This analysis focused on isoprene and monoterpenes as they are known contributors to SOA production and part of the goal of this study was to look at the effect of BVOC and anthropogenic oxidants on growth rate. Little correlation was found between the concentration of these gases and the magnitude of the peak growth rate, though it should be noted that there was no gas data available for many of the days and that a pattern may have been found with a more complete data set.

			at peak				at sunset	
	approx. peak time	peak GR (nm/hr)	NO_3 (ppb)	ozone (ppb)	monoterpenes (ppb)	isoprene (ppb)	monoterpenes (ppb)	isoprene (ppb)
24-Jul	10:00 PM	7.87	3.56E-03	19.47	1.92	2.00	1.38	2.50
27-Jul	9:30 PM	4.60	ND	13.96	ND	ND	ND	ND
28-Jul	9:00 PM	8.11	ND	11.58	ND	ND	ND	ND
29-Jul	9:30 PM	18.64	ND	11.84	ND	ND	ND	ND
30-Jul	9:00 PM	10.17	ND	15.38	ND	ND	ND	ND
31-Jul	12:00 AM	20.97	1.88E-03	12.63	4.73	6.79	1.81	7.93
2-Aug	11:00 PM	25.63	1.02E-02	34.83	-0.44	3.69	4.37	7.51
3-Aug	11:40 PM	15.83	3.16E-03	20.61	1.11	0.70	1.51	7.44
4-Aug	10:30 PM	5.29	2.02E-03	23.10	0.70	1.01	0.79	1.73
9-Aug	8:00 PM	5.22	2.88E-03	60.17	ND	ND	ND	ND
10-Aug	9:45 PM	6.61	5.42E-03	35.50	ND	ND	ND	ND
24-Aug	11:15 PM	6.96	ND	12.95	5.77	1.00	5.99	3.87
27-Aug	8:00 PM	6.59	ND	28.39	3.18	8.97	4.56	6.48

Table 2: Mixing ratios of relevant gases at the time of peak growth rate and at sunset. Days on which a negative growth rate was observed between the hours of 7 PM and 9 PM are highlighted in yellow

The following dataset is an example of a day (July 24th) on which no negative growth rate was observed in the evening hours, despite a gradual decrease in both the concentration of oxidants and SOA precursor gases. Figure 9 shows that there was a peak in the growth rate at around 10 PM. Analysis of the VOC concentrations (Figure 10) shows that there was a high mixing ratio of isoprene in the hours preceding sunset, which was at 8:19 PM. The mixing ratio of ozone slowly tapered off after a peak around 6:30 PM, but remained high (above 10 ppb) until after 3 AM (Figure 10). Nitrate radical mixing ratios estimated using Equation 7 also decreased into the night. There was a brief period of negative growth rate just before 6 AM, which coincided with low oxidant gas mixing ratios. While isoprene concentrations were low, the concentration of monoterpenes was high during the particle shrinkage period.

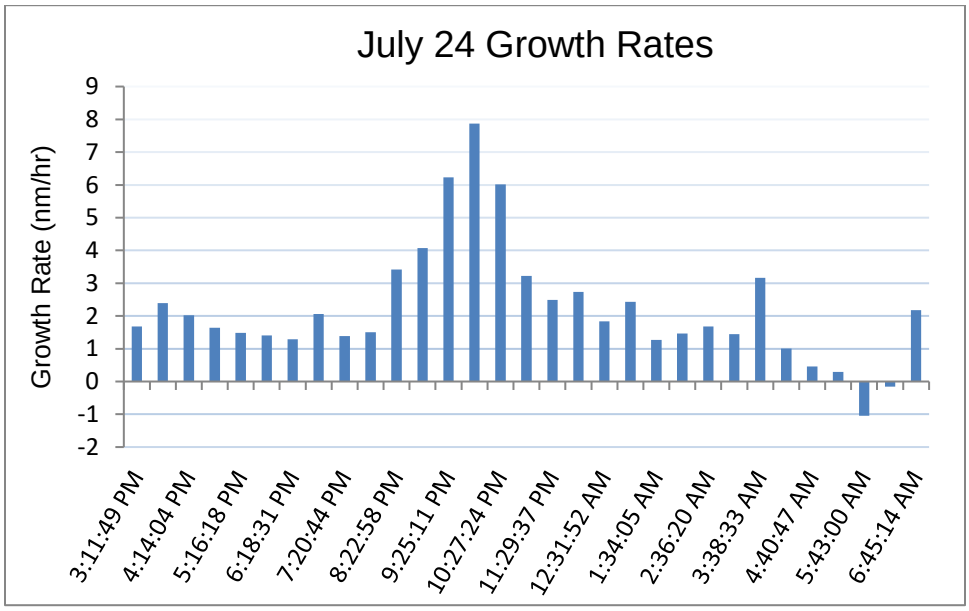

Figure 9: Growth rate of tracked mode aerosol from an experiment conducted on July 24, 2015 under exposure to ambient gas concentrations

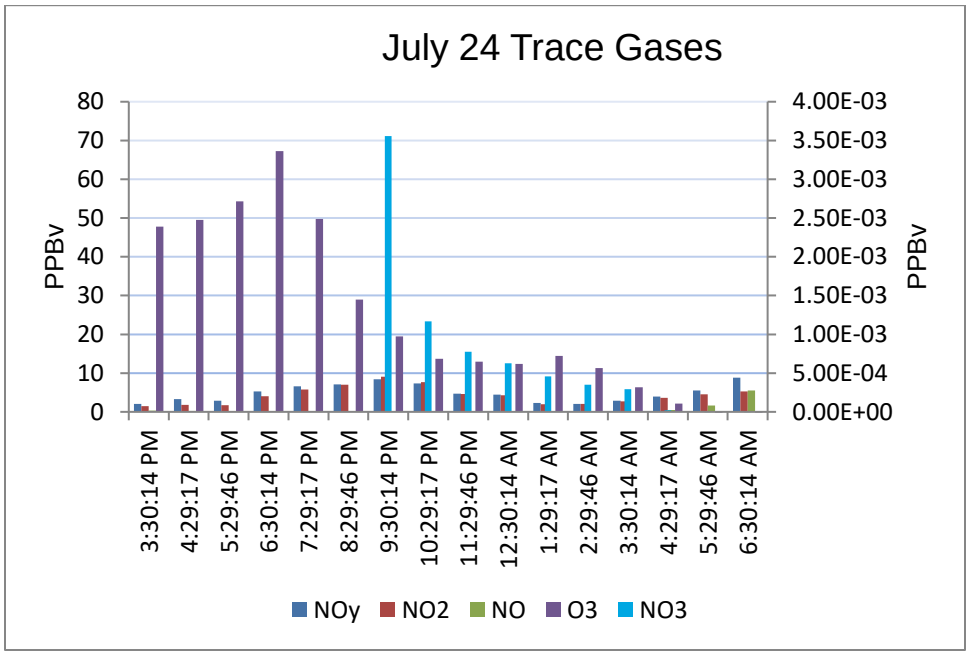

Figure 10: Trace gas concentrations for July 24, 2015. The calculated approximate NO_3 mixing ratio is in relation to the right y-axis, all other gas concentrations are in relation to the left y-axis. NO_3 concentration was only calculated for measurements taken after sunset.

Time	Methanol	Acetaldehyde	Acetone	Isoprene	MVK/Pentene	MEK/Butanal	Benzene	Toluene	Xylenes	TMB	Monoterpenes
3:30 PM	14.91	1.60	3.17	4.67	1.84	0.89	0.33	2.24	1.63	0.42	0.61
4:29 PM	14.22	1.64	3.59	6.73	1.86	1.06	0.29	0.38	0.21	0.36	0.60
5:29 PM	13.64	1.62	3.56	6.00	1.67	0.93	0.34	0.43	0.18	0.23	0.71
6:30 PM	15.99	2.70	4.92	7.23	2.35	1.52	0.75	0.58	0.30	0.36	0.89
7:29 PM	18.96	3.61	5.71	4.50	2.92	1.81	1.01	0.66	0.51	0.44	0.96
8:29 PM	16.76	2.59	3.83	2.50	2.20	1.23	0.57	0.66	0.47	0.43	1.38
9:30 PM	17.11	2.39	3.67	2.00	1.69	1.13	0.55	0.85	0.58	0.42	1.92
10:29 PM	15.28	1.93	3.20	1.48	1.36	0.85	0.45	0.76	0.52	0.49	2.06
11:29 PM	9.35	1.02	2.08	1.48	0.79	0.49	0.31	0.30	0.29	0.33	1.08
12:30 AM	7.91	0.79	1.85	1.14	0.44	0.44	0.17	0.32	0.20	0.29	0.98
1:29 AM	5.94	0.61	1.57	0.59	0.21	0.42	0.22	0.32	0.17	0.25	1.03
2:29 AM	4.95	0.63	1.73	0.45	0.19	0.38	0.17	0.37	0.13	0.32	1.36
3:30 AM	4.80	0.62	2.48	0.60	0.14	0.33	0.19	0.32	0.17	0.34	2.88
4:29 AM	4.13	0.55	2.93	0.60	0.19	0.42	0.22	0.46	0.27	0.33	3.62
5:29 AM	2.95	0.43	2.85	0.66	0.22	0.35	0.24	0.50	0.20	0.38	4.40
6:30 AM	3.32	0.34	3.40	0.67	0.14	0.31	0.23	0.55	0.34	0.31	4.76

Figure 11: Hourly averaged PTR-MS gas concentrations for July 24, 2015

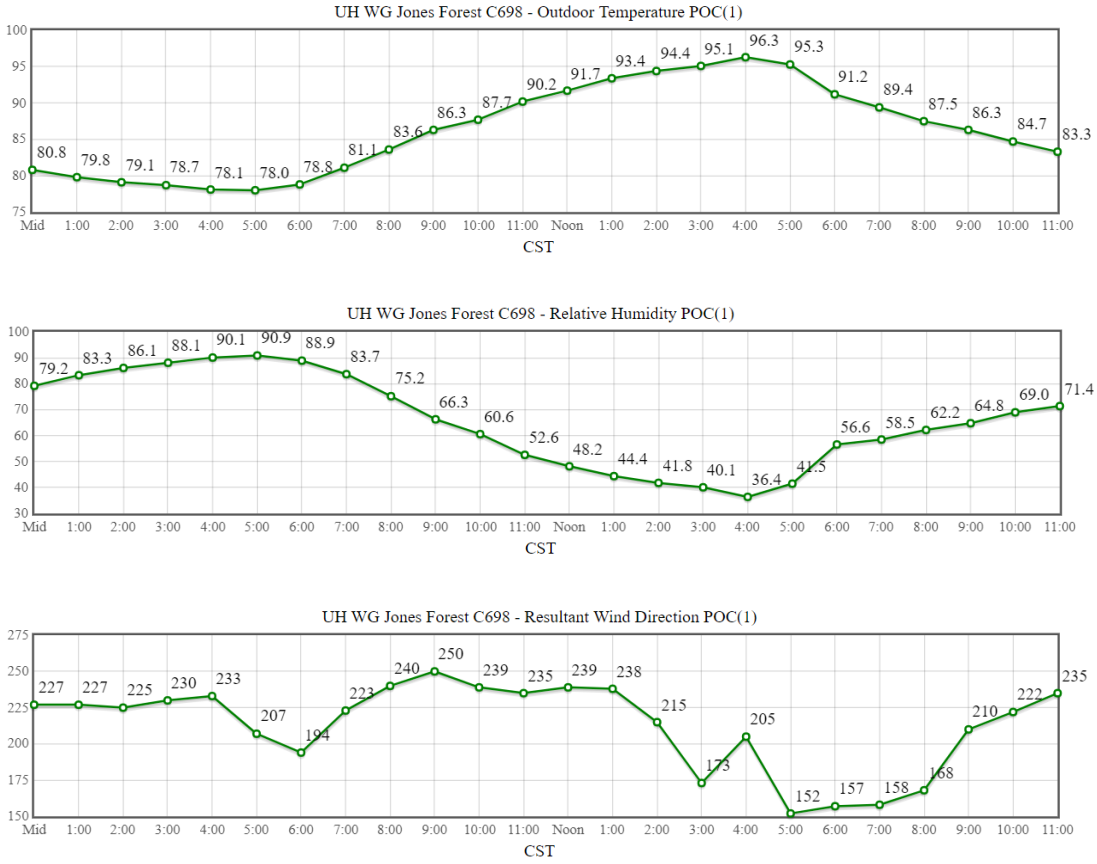

Figure 12: Temperature, relative humidity and wind direction graphs for July 24, 2015 in Conroe, TX. Reprinted from the Texas Commission on Environmental Quality.

On July 31 there was a significant peak in growth rate around 12 AM (~21 nm/hr). Trace gas concentrations were not available before 6:30 PM due to instrument maintenance. Estimated nitrate radical and measured ozone concentrations were high between 12:30 and 1:30 AM (3.3 x 10^{-3} ppb and 15.3 ppb, respectively). Isoprene mixing ratios stayed high late into the evening. Monoterpene concentrations were low until about 8:30 PM, when they began to increase significantly, reaching a peak at around

11:30 PM (Figure 15). The peaks in growth rate seem to track the peaks in oxidant (ozone and nitrate radical) concentrations, with a minimum in both oxidants at about 10 PM, and a minimum in growth rate at about 10:30 PM. Low relative humidity (27.3% to 29.1%) and high temperature (90.5° F to 95.8° F) in the early evening could have contributed to the low growth rate before sunset. Very little particle shrinkage was observed, which may be due to the fact that the concentrations of both oxidants and VOCs (monoterpenes in particular) stayed high into the early morning hours.

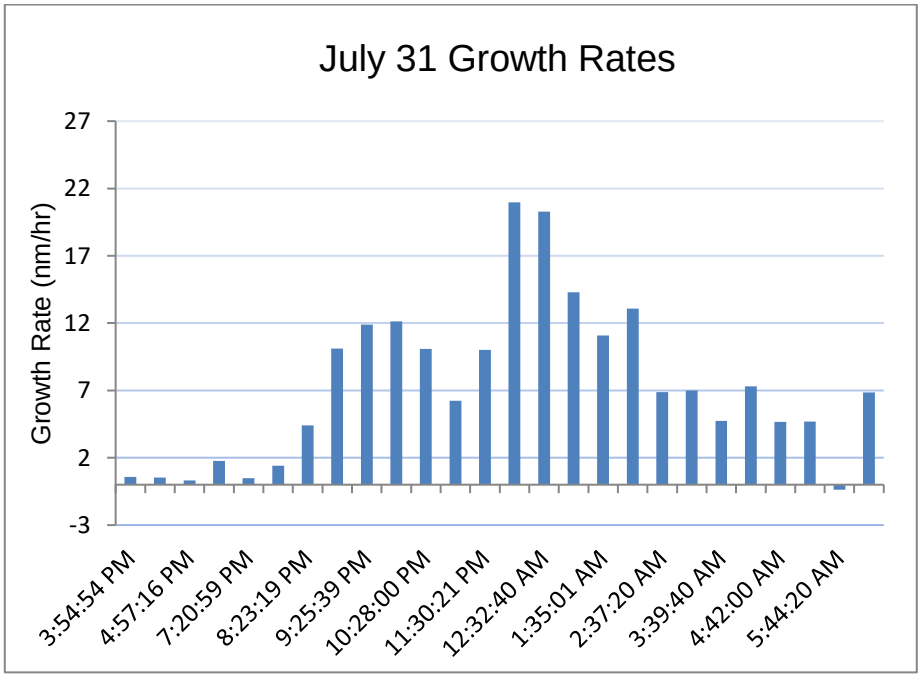

Figure 13: Growth rate of tracked mode aerosol from an experiment conducted on July 31, 2015 under exposure to ambient gas concentrations

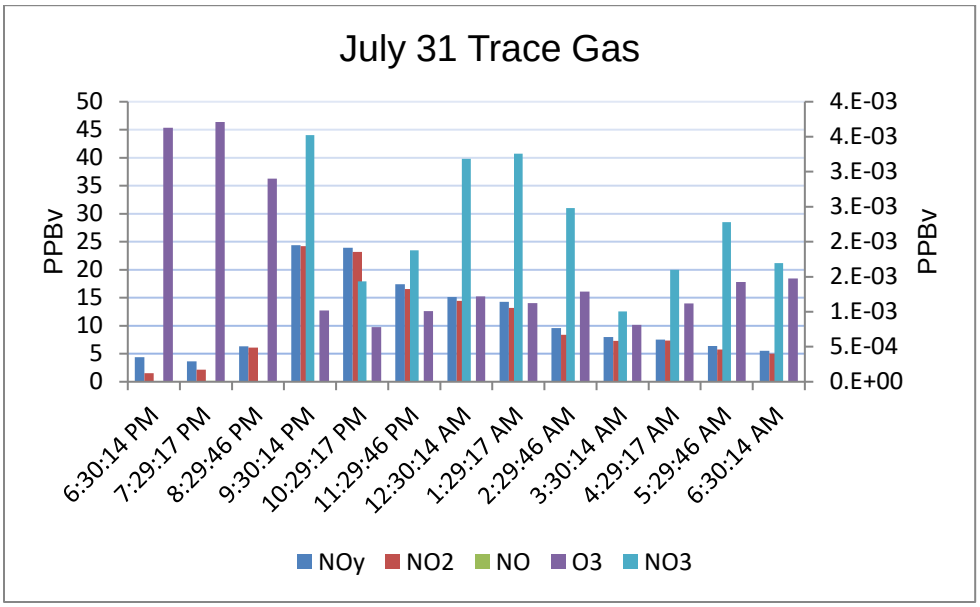

Figure 14: Trace gas concentrations for July 31, 2015. The calculated approximate NO_3 mixing ratio is in relation to the right y-axis, all other gas concentrations are in relation to the left y-axis. NO_3 concentration was only calculated for measurements taken after sunset.

Time	Methanol	Acetaldehyde	Acetone	Isoprene	MVK/Pentene	MEK/Butanal	Benzene	Toluene	Xylenes	TMB	Monoterpenes
2:29 PM	36.72	3.08	5.39	8.28	2.99	1.54	-0.40	0.10	-0.08	-0.04	-1.24
3:30 PM	35.28	2.62	5.29	8.39	2.41	1.32	-0.22	0.13	-0.01	-0.09	-1.14
4:29 PM	32.74	2.38	4.77	8.46	2.26	1.08	-0.25	0.13	-0.02	-0.04	-1.14
5:29 PM	27.91	2.12	4.02	7.76	2.38	0.74	-0.21	0.12	0.24	0.08	-1.12
6:30 PM	30.23	2.44	4.21	9.15	2.90	0.87	-0.04	0.31	0.29	0.04	-0.75
7:29 PM	31.82	2.78	4.45	8.40	3.48	0.99	0.01	0.50	0.39	0.08	-0.51
8:29 PM	42.52	3.88	6.69	7.93	4.46	1.63	0.31	1.12	0.80	0.40	1.81
9:30 PM	54.32	4.81	8.86	8.40	4.94	2.06	0.66	1.60	1.20	0.62	3.99
10:29 PM	58.88	5.44	9.42	7.77	5.10	2.24	0.80	1.65	1.36	0.68	4.35
11:29 PM	53.35	5.55	10.02	6.79	5.00	2.25	0.90	1.66	1.25	0.69	4.73
12:30 AM	44.23	4.99	9.57	4.50	4.20	2.21	0.59	1.30	1.09	0.64	3.68
1:29 AM	38.34	4.20	9.42	3.38	3.34	1.83	0.72	1.45	1.11	0.67	3.68
2:29 AM	31.63	3.60	8.98	2.56	2.84	1.63	0.65	1.33	1.01	0.68	3.19
3:30 AM	26.51	3.41	9.48	2.84	2.30	1.56	0.50	2.04	1.24	0.78	3.20
4:29 AM	23.16	2.92	8.13	1.86	2.11	1.31	0.56	1.45	1.36	0.74	2.23
5:29 AM	22.94	2.51	6.95	1.43	1.84	1.23	0.60	1.46	1.21	0.60	1.34
6:30 AM	33.87	4.16	10.09	1.61	3.18	1.82	0.96	2.06	1.64	0.95	4.52

Figure 15: Hourly averaged PTR-MS gas concentrations for July 31, 2015

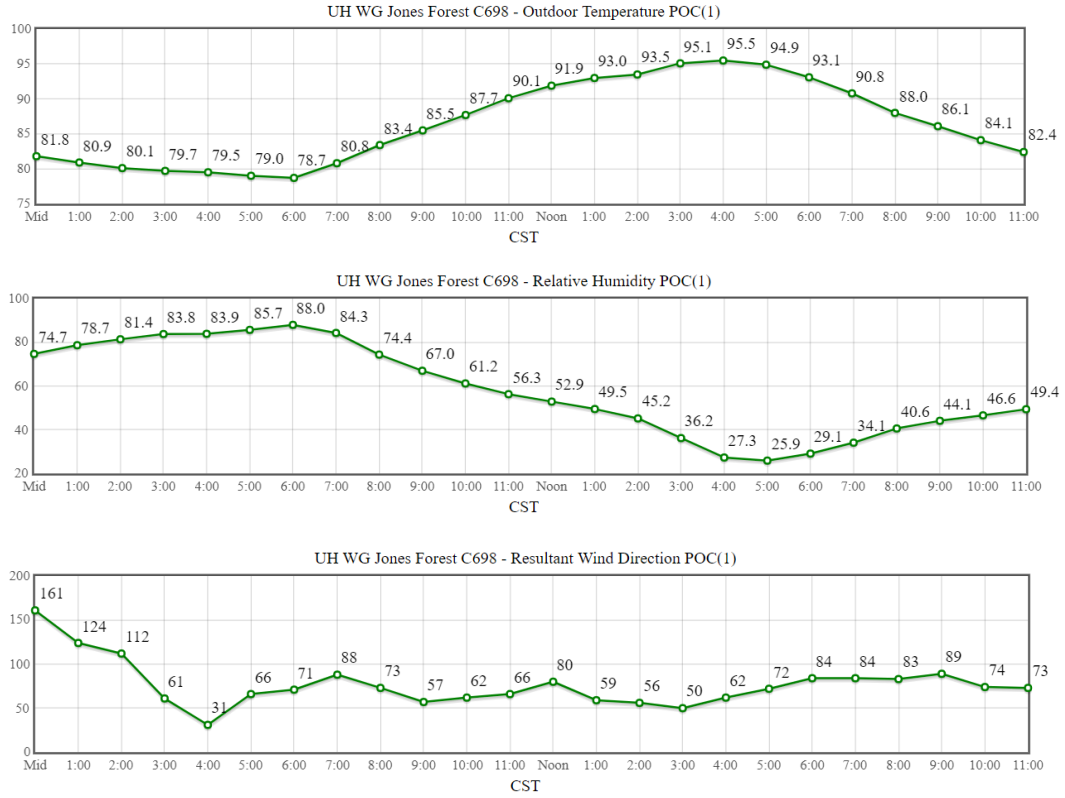

Figure 16: Temperature, relative humidity and wind direction graphs for July 31, 2015 in Conroe, TX. Reprinted from the Texas Commission on Environmental Quality.

On August 1st, a high concentration of ozone and a high concentration of isoprene in the pre-sunset hours were measured. Measurements of growth rate were not available after 12 AM, but a steady increase culminating in a high growth rate of 25 nm/hr was observed leading up to that point (Figure 18). Monoterpene concentrations were high after 9:30 PM (Figure 19). The peak in growth rate occurred about 1 hour after a peak in nitrate radical concentration, which coincided with a high concentration of isoprene (9.3 ppb). The oxidation byproducts of the reaction between isoprene and nitrate radical are known to be more volatile, and would therefore be more responsive to

changes in atmospheric dilution and could result in a less stable aerosol (Ng *et al.*, 2007). However, without growth rate data from a time period where the concentration of oxidant and VOC gases had decreased significantly, it is not possible to know the stability of this aerosol population. Similar to the previous night, low relative humidity and high temperatures before sunset could have contributed to the low growth rates observed around this time (Figure 20). There was a significant concentration of both oxidant gases and VOCs throughout the observed growth rate period, which likely contributed to the high growth rate observed.

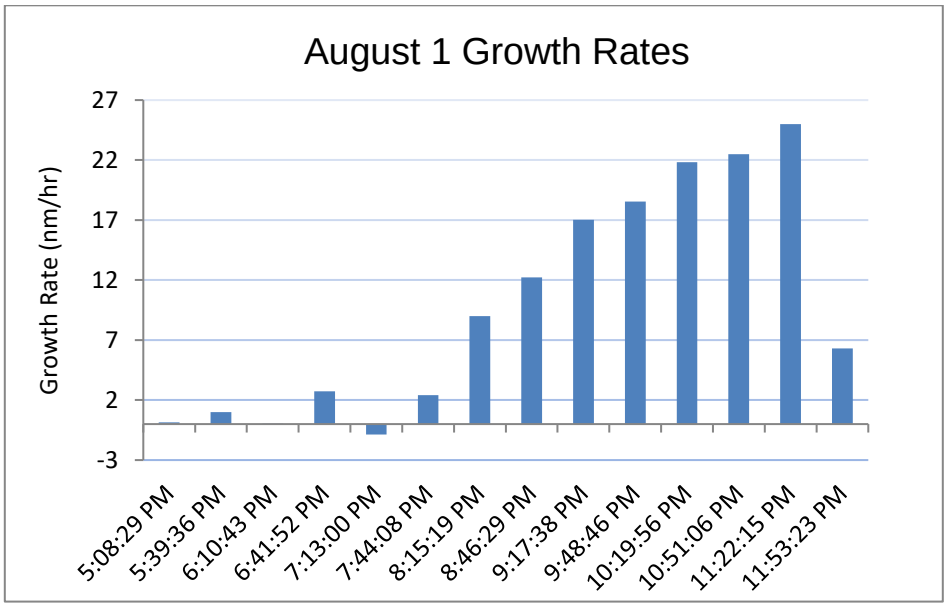

Figure 17: Growth rate of tracked mode aerosol from an experiment conducted on August 1, 2015 under exposure to ambient gas concentrations

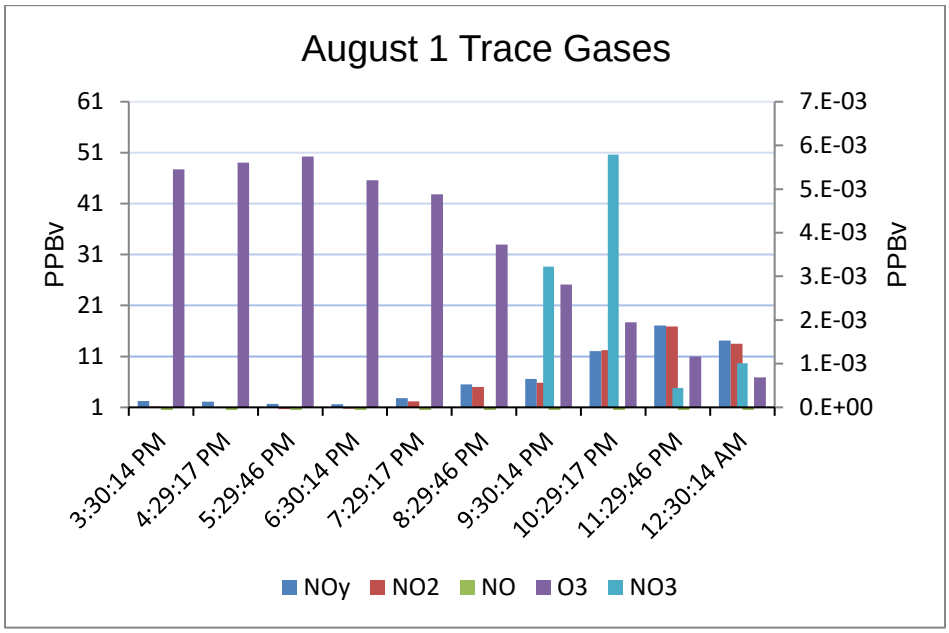

Figure 18: Trace gas concentrations for August 1, 2015. The calculated approximate NO_3 mixing ratio is in relation to the right y-axis, all other gas concentrations are in relation to the left y-axis. NO_3 concentration was only calculated for measurements taken after sunset.

Time	Methanol	Acetaldehyde	Acetone	Isoprene	MVK/Pentene	MEK/Butanal	Benzene	Toluene	Xylenes	TMB	Monoterpenes
3:30:14 PM	30.72	2.31	4.20	7.16	3.53	1.05	-0.18	0.26	0.24	0.01	-0.96
4:29:17 PM	30.13	2.52	4.55	6.47	3.67	1.21	0.19	0.47	0.35	0.18	-0.77
5:29:46 PM	29.98	2.48	4.78	6.55	3.40	1.25	0.31	0.49	0.43	0.24	-0.63
6:30:14 PM	30.71	2.32	4.13	7.79	2.72	0.94	0.47	0.57	0.62	0.34	-0.21
7:29:17 PM	32.79	2.67	4.54	8.21	3.08	1.15	0.69	0.94	0.91	0.56	0.33
8:29:46 PM	46.90	3.92	7.18	7.51	4.19	1.81	0.72	1.15	0.88	0.55	2.25
9:30:14 PM	56.49	4.97	9.51	8.25	4.74	2.32	0.96	1.93	1.37	0.83	4.37
10:29:17 PM	53.78	5.00	9.66	9.32	4.84	2.17	1.31	2.42	1.61	1.06	5.10
11:29:46 PM	50.69	5.36	10.10	8.84	4.76	2.13	1.31	2.95	1.89	1.04	5.74
12:30:14 AM	47.27	5.31	11.44	8.35	4.43	2.27	1.35	3.12	1.86	0.83	6.24

Figure 19: Hourly averaged PTR-MS gas concentrations for August 1, 2015

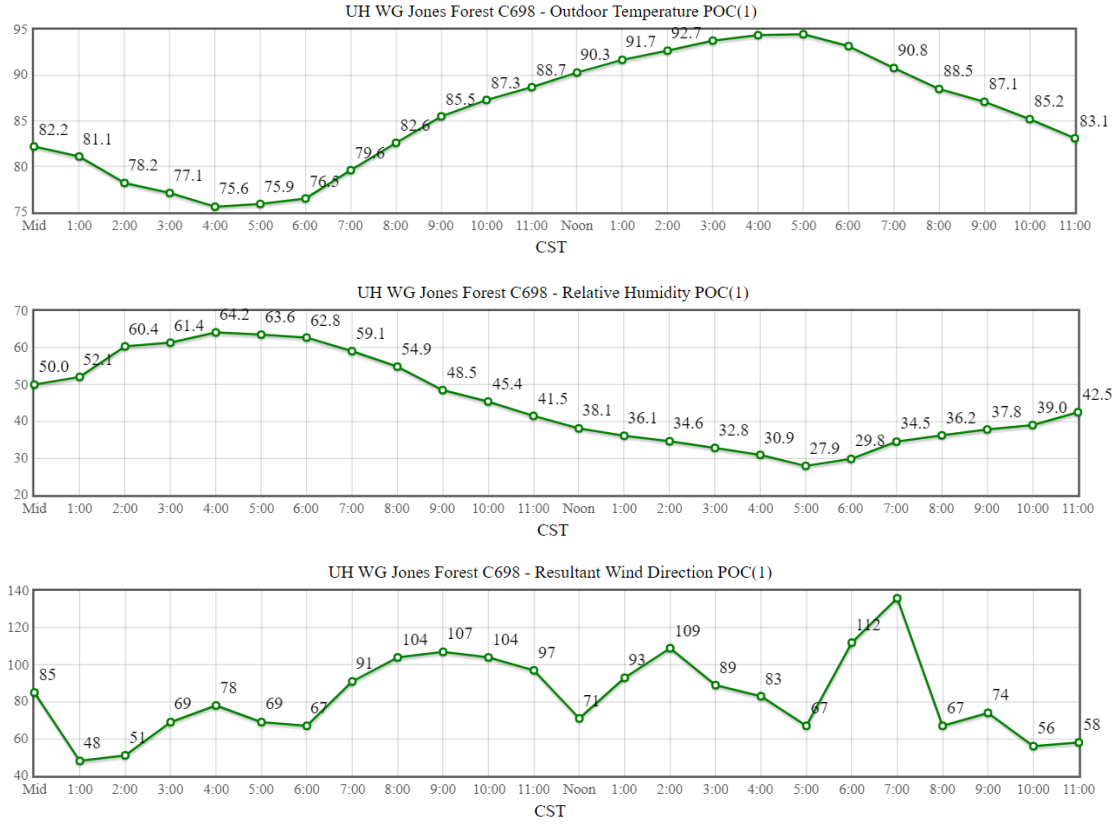

Figure 20: Temperature, relative humidity and wind direction graphs for August 1, 2015 in Conroe, TX. Reprinted from the Texas Commission on Environmental Quality.

August 3rd exhibited two peaks in growth rate, followed by a period of particle evaporation in the early morning hours (Figure 21). There was a slight decrease in the mixing ratio of ozone at around 8:30 PM, followed by an increase in estimated nitrate radical mixing ratio with a peak at about 10:30 PM (Figure 22). The two peaks in growth rate are offset from these two features in the oxidant concentrations by about 1 hour; the minimum value between the growth rate peaks is achieved at approximately 9:30 PM, while the maximum value of the sequential peak occurs at about 11:40 PM. There was a

high concentration of isoprene before sunset that decreased to < 1 ppb by 10:30 PM (Figure 23). Monoterpene concentrations began to climb after 10:30 PM. The temperature dropped and the relative humidity climbed after sunset, from 86.7° F and 56.8% at sunset to 82.4° F and 70.5% at midnight, which could have contributed to the peak in growth rate (Figure 24). There was a marked period of particle shrinkage between 4 AM and 6 AM, which coincided with a minimum in both the ozone and estimated nitrate radical mixing ratios. The mixing ratio of monoterpenes was fairly high at this point, suggesting that the oxidant mixing ratio is the rate-limiting factor in the production of gases leading to SOA growth.

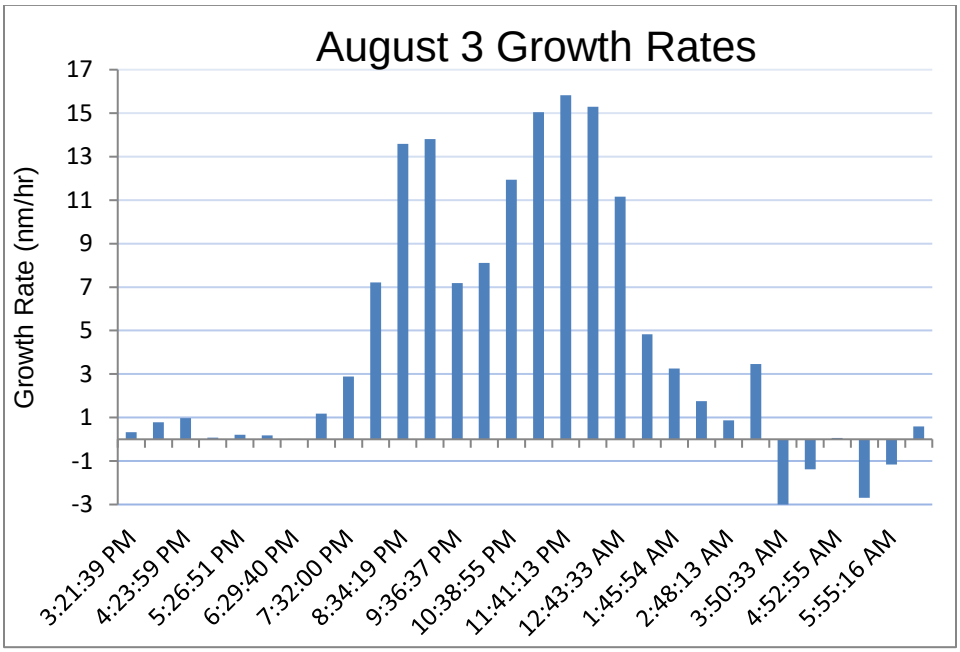

Figure 21: Growth rate of tracked mode aerosol from an experiment conducted on August 3, 2015 under exposure to ambient gas concentrations

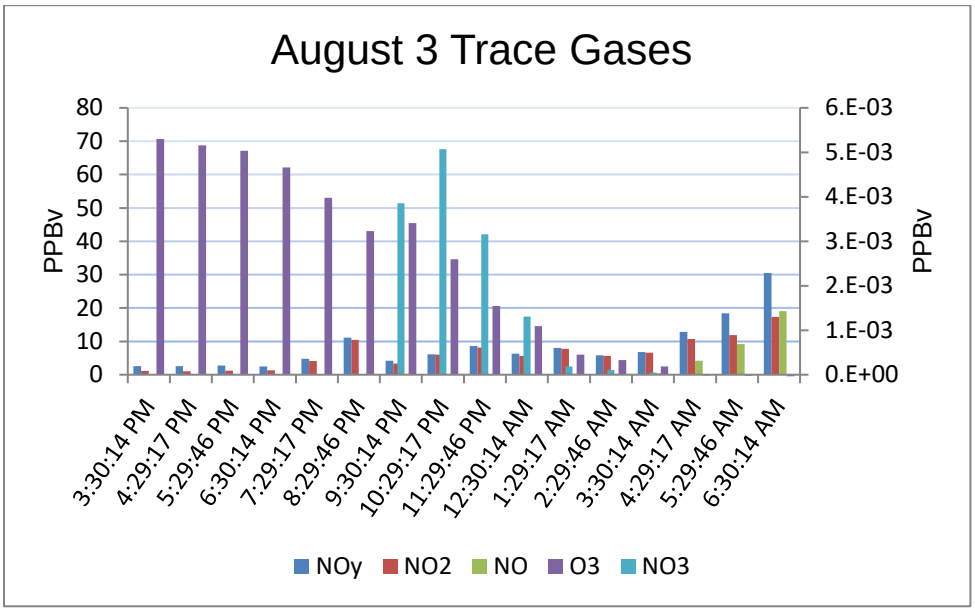

Figure 22: Trace gas concentrations for August 3, 2015. The calculated approximate NO_3 mixing ratio is in relation to the right y-axis, all other gas concentrations are in relation to the left y-axis. NO_3 concentration was only calculated for measurements taken after sunset.

Time	Methanol	Acetaldehyde	Acetone	Isoprene	MVK/Pentene	MEK/Butanal	Benzene	Toluene	Xylenes	TMB	Monoterpenes
2:29:46 PM	28.03	2.32	5.49	3.70	2.09	1.62	0.63	1.15	0.75	0.54	-0.46
3:30:14 PM	27.62	2.48	5.43	4.71	2.41	1.52	0.77	1.49	0.90	0.43	-0.32
4:29:17 PM	26.82	2.55	5.47	5.05	2.33	1.65	0.47	1.47	0.83	0.50	-0.40
5:29:46 PM	28.44	2.68	5.40	5.64	2.86	1.29	0.65	0.81	0.58	0.52	-0.35
6:30:14 PM	31.43	2.79	5.71	7.91	2.99	1.45	0.95	1.18	1.00	0.81	0.17
7:29:17 PM	37.09	3.09	6.27	9.19	3.08	1.64	1.14	1.29	1.25	0.94	0.77
8:29:46 PM	44.83	4.24	7.90	7.44	3.64	2.20	1.52	1.55	1.56	1.03	1.51
9:30:14 PM	24.32	2.37	5.38	1.08	0.63	1.21	1.29	1.44	1.23	0.99	0.60
10:29:17 PM	28.98	2.68	5.87	0.70	0.48	1.13	1.32	1.60	1.35	1.21	1.11
11:29:46 PM	32.16	3.28	8.23	0.94	0.51	1.52	1.29	1.56	1.22	1.12	2.74
12:30:14 AM	28.03	3.10	8.44	1.01	0.62	1.53	1.49	2.12	1.64	1.41	3.17
1:29:17 AM	19.13	2.44	7.13	1.17	0.40	1.19	1.11	1.76	1.45	1.17	3.95
2:29:46 AM	15.48	1.97	6.31	1.27	0.43	0.97	1.18	1.81	1.31	1.33	3.64
3:30:14 AM	16.68	1.98	6.73	1.12	0.41	0.82	1.32	1.86	1.35	1.21	4.29
4:29:17 AM	14.71	1.55	5.89	1.05	0.24	0.99	1.28	1.69	1.31	1.12	4.95
5:29:46 AM	13.85	1.41	5.31	1.11	0.20	0.64	1.09	1.71	1.37	1.22	5.29
6:30:14 AM	13.85	1.41	5.31	1.11	0.20	0.64	1.09	1.71	1.37	1.22	5.29

Figure 23: Hourly averaged PTR-MS gas concentrations for August 3, 2015

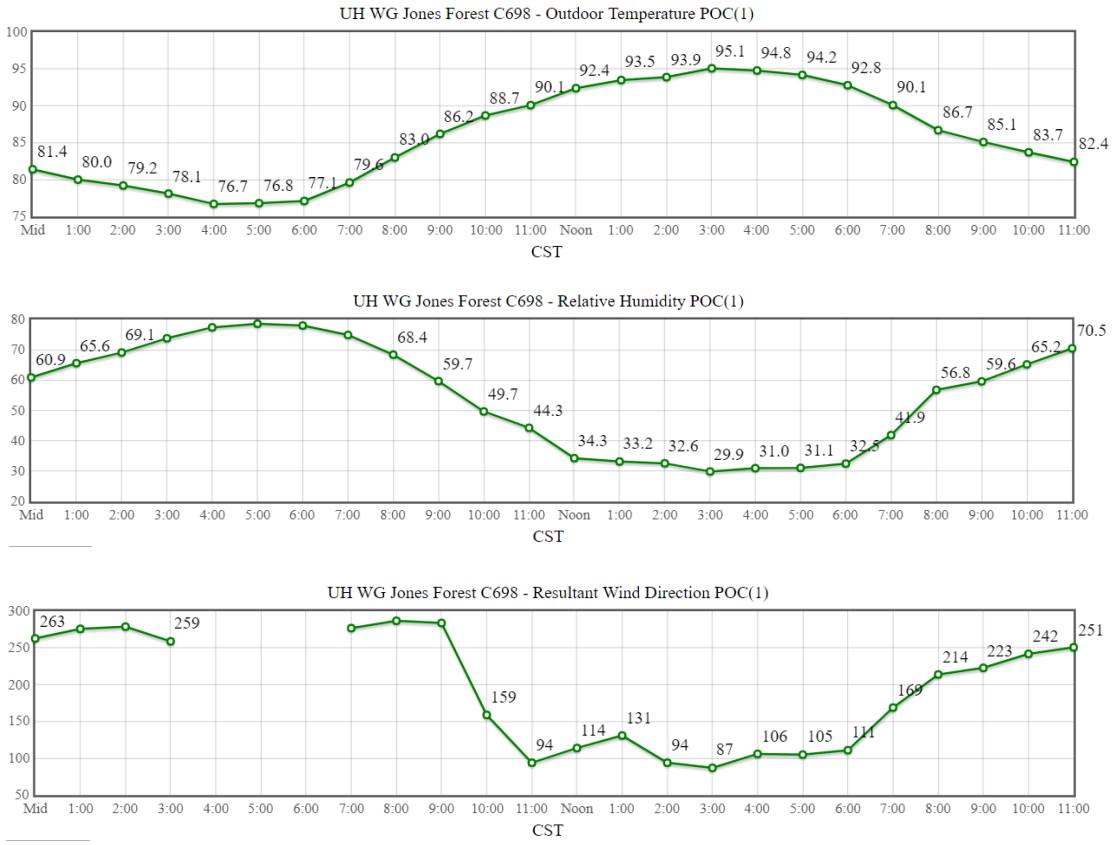

Figure 24: Temperature, relative humidity and wind direction graphs for August 3, 2015 in Conroe, TX. Reprinted from the Texas Commission on Environmental Quality.

The highest particle growth rates were observed on August 2nd (Figure 25). There was a high ozone mixing ratio in the afternoon (> 50 ppb) and leading into the early evening (Figure 26). There was a brief drop in ozone concentration at around 9:30 PM, which may be correlated to the slight decrease in growth rate at about 10:40 PM. After this period the ozone mixing ratio increased to about 45 ppb before slowly decreasing to 3 ppb by 5:30 AM. There was a peak in nitrate radical concentration corresponding to the 2nd peak in ozone mixing ratio between 10:30 and 11:30 PM. The

isoprene mixing ratio was high (3-7 ppb) until about 11:30 PM when it dropped to about 1 ppb (Figure 27). While there was a period of high monoterpene mixing ratio before the peak in growth rate (1.5 – 3 ppb between 8:30 and 10:30 PM), the predominant VOC before 11:30 PM was isoprene. After 12:30 AM, the mixing ratio of monoterpenes increased, staying high (>3 ppb) for the rest of the night. If the peak in particle growth rate was controlled by the mixing ratio of oxidant gases, then it would have been expected that a peak in growth rate would have followed the peaks in both ozone and nitrate radical at 11:30 PM. However, this time period also corresponds to a minimum in the concentrations of both isoprene and monoterpenes, indicating that the growth rate is not entirely dependent on the concentration of oxidant gases. An unusual feature of this day was a predominantly north/northeasterly wind in the hours preceding sunset, with wind direction from due east between 7 PM and 7:30 PM (Figure 28). This could have brought in an air mass from a different region than that observed on previous nights. A NOAA HYSPLIT model run for this location and time show that through the late evening, air is coming into the region predominantly from East Texas (Figure 29). There could be VOCs in this air mass that are not measured by the PTR-MS contributing to high growth rates.

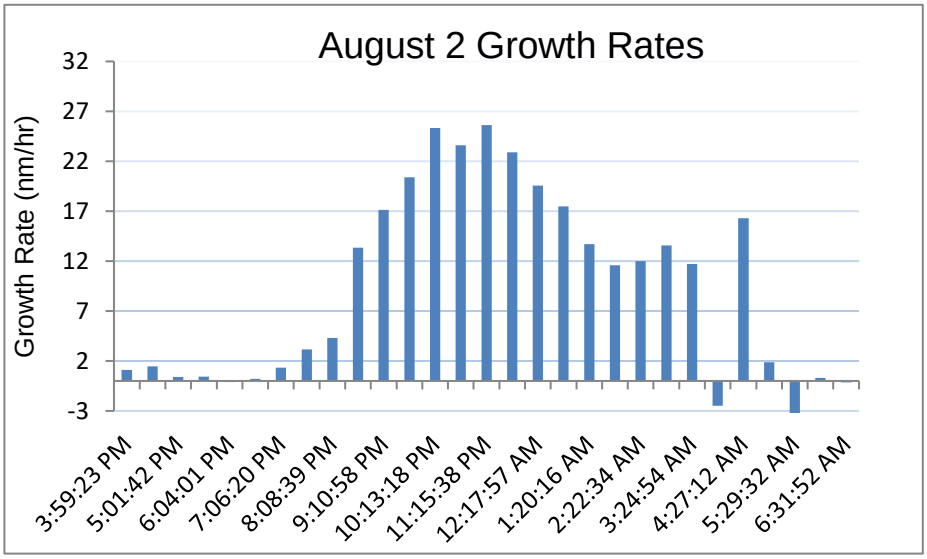

Figure 25: Growth rate of tracked mode aerosol from an experiment conducted on August 2, 2015 under exposure to ambient gas concentrations

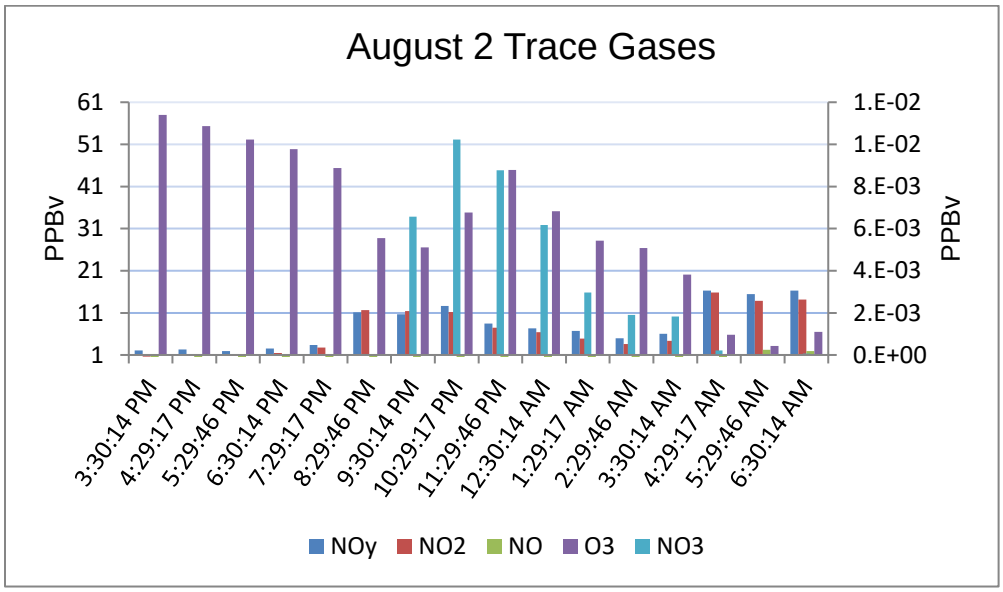

Figure 26: Trace gas concentrations for August 2, 2015. The calculated approximate NO_3 mixing ratio is in relation to the right y-axis, all other gas concentrations are in relation to the left y-axis. NO_3 concentration was only calculated for measurements taken after sunset.

Time	Methanol	Acetaldehyde	Acetone	Isoprene	MVK/Pentene	MEK/Butanal	Benzene	Toluene	Xylenes	TMB	Monoterpenes
2:29:46 PM	27.06	2.44	4.30	4.39	2.50	1.04	0.16	0.62	0.61	0.07	-0.94
3:30:14 PM	27.16	2.39	4.48	4.13	2.60	1.08	0.29	0.50	0.63	0.26	-1.09
4:29:17 PM	28.45	2.52	4.49	5.23	2.61	1.07	0.22	0.55	0.51	0.35	-0.82
5:29:46 PM	29.19	2.56	4.60	6.02	2.91	1.18	0.26	0.61	0.46	0.24	-0.72
6:30:14 PM	32.20	2.98	4.84	6.45	3.37	1.42	0.72	0.68	0.96	0.36	-0.33
7:29:17 PM	34.05	3.10	5.27	6.63	3.36	1.43	0.81	0.86	0.86	0.55	0.20
8:29:46 PM	50.30	4.55	7.72	7.53	4.13	1.96	1.05	1.22	1.20	0.75	1.78
9:30:14 PM	51.40	4.89	8.99	5.98	3.90	2.35	0.96	1.33	1.26	1.06	2.96
10:29:17 PM	48.60	5.32	9.69	2.97	2.61	2.43	1.34	1.62	1.53	1.21	1.59
11:29:46 PM	40.63	4.48	9.09	1.12	1.18	2.06	1.24	1.31	1.32	1.07	1.08
12:30:14 AM	40.72	4.93	11.25	1.13	1.09	2.12	1.34	1.54	1.41	1.06	2.23
1:29:17 AM	35.93	4.48	11.93	1.04	1.03	2.11	1.31	1.65	1.33	0.89	3.06
2:29:46 AM	33.80	4.13	11.53	0.88	0.73	2.10	1.20	1.69	1.44	1.03	3.42
3:30:14 AM	30.58	3.88	12.08	1.33	0.92	1.89	1.13	1.67	1.27	0.96	3.32
4:29:17 AM	21.80	3.20	11.76	1.26	0.75	1.57	1.20	1.87	1.45	1.10	4.41
5:29:46 AM	18.99	2.54	10.88	1.40	0.45	1.34	1.13	2.03	1.39	1.04	4.26
6:30:14 AM	16.70	2.29	10.30	0.94	0.44	1.23	1.27	1.92	1.40	1.19	4.07

Figure 27: Hourly averaged PTR-MS gas concentrations for August 2, 2015

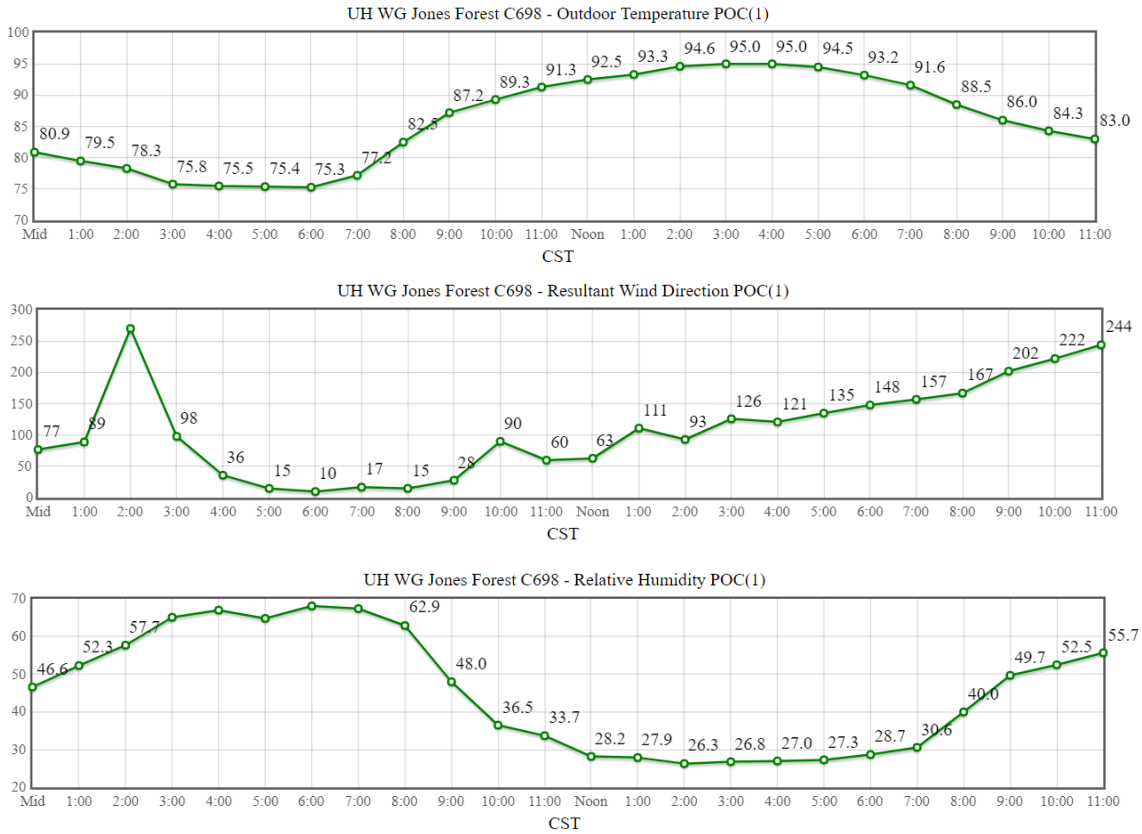

Figure 28: Temperature, relative humidity and wind direction graphs for August 2, 2015 in Conroe, TX. Reprinted from the Texas Commission on Environmental Quality.

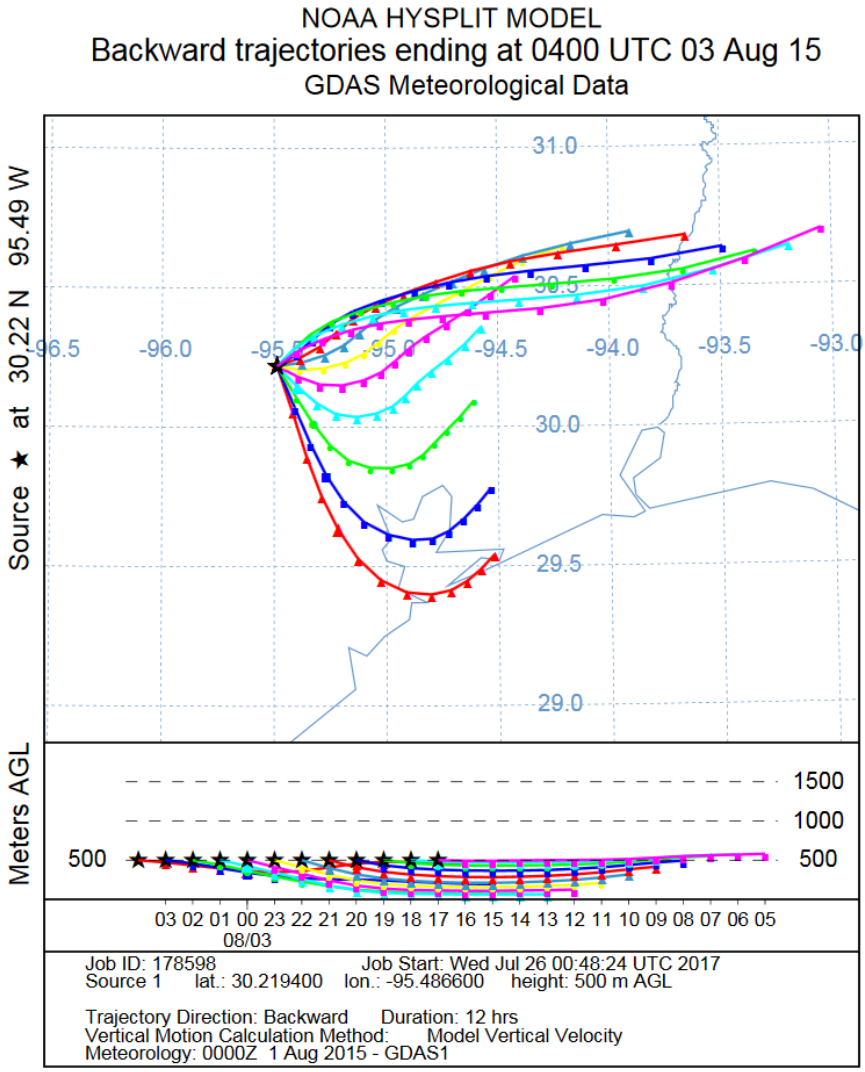

Figure 29: NOAA HYSPLIT backtrajectory model of the W G Jones State Forest the evening of August 2, 2015. Reprinted from the National Oceanic and Atmospheric Association, Air Resources Laboratory.

Two trends in particle shrinkage were examined – shrinkage after sunset and shrinkage in the early morning hours when the concentrations of organic compounds more prone to oxidation had decreased significantly. A factor that might be expected to

contribute to a negative growth rate at sunset is the decrease in ozone concentration that typically occurs as its primary production pathway (the photolysis of NO_2) is cut off. However, the decrease in ozone concentration in this study frequently occurred very gradually after sunset, and there was often an appreciable amount of ozone left over well past midnight. On most days a significant decrease in growth rate after sunset was not observed, indicating that either the aerosol formed was relatively stable and non-volatile, or that some other process was contributing to particle growth.

Concentrations of ozone, nitrate radical, isoprene and monoterpenes were the main parameters examined for correlations with the aerosol size stability. Some trends were observed tying high concentrations of oxidants and VOCs to higher growth rates. Days with periods of high growth rate (>15 nm/hr) were correlated with high oxidant and VOC mixing ratios occurring within 1 hour before the peak. Considering that the exchange time for ambient air into the CAGE chamber is on the order of 30 minutes, and gas measurements were averaged over every hour, it is reasonable to assume that the oxidation of either isoprene or monoterpenes was responsible for the high growth rates. This effect was particularly evident on July 31, when two peaks in growth rate were observed that seemed to track similar peaks in the oxidant gas mixing ratios, offset by about 1 hour. Concentrations of both isoprene and monoterpenes were both high and fairly constant through both of these periods. July 31 was also unique in that very little particle evaporation was observed. This may be attributable to the concentration of oxidant gases that stayed unusually high throughout the night. Days on which low growth rates were observed typically had lower concentrations of both oxidant gases and

VOCs (for example, July 24). August 2 and 3 both had very high growth rates, and both exhibited significant particle shrinkage (< -1nm/hr) in the early morning hours. Both of these days also had periods of high nitrate radical mixing ratio coupled with periods of high monoterpene concentrations, which could indicate that the particle evaporation was associated with the oxidation byproducts of these two gases. However, the magnitude of this response was not in proportion to the magnitude of the growth rate when high concentrations of the relevant gases were present, indicating that the aerosol formed is relatively stable and that the condensed products are somehow changed to no longer be responsive to changes in the concentration of their gaseous counterparts.

CHAPTER V

CONCLUSIONS

These experiments showed evidence of limited early morning evaporation of particles that had grown during nighttime gas-to-particle conversion. This trend might be due to the typical decrease in concentrations of oxidant gases as nighttime progresses, but more information is needed to determine the cause of the change in particle size. Temperature and relative humidity do not seem to be likely contributors to this effect, as measurements from nearby Conroe show that the early morning hours were often cooler and more humid than earlier in the evening. If the newly-condensed species were in equilibrium with their vapor-phase counterparts, it would be expected that a decrease in the concentration of vapor-phase species would cause a decrease in the mass of the particle population as the condensed species re-volatilize to maintain equilibrium. While this does appear to occur, the extent of the particle shrinkage is not proportional to the decrease in ambient gas concentration measured by the PTR-MS and trace gas analyzers. This suggests that the condensed species might have undergone further processing after condensation onto the particles, and are therefore no longer in equilibrium with the vapor phase. If the species remained chemically unchanged after condensation, the growth rate would more closely mirror the rate of change of concentrations of BVOC and oxidants, and the magnitude of the particle shrinkage would be comparable to the magnitude of particle growth earlier in the evening.

Future experiments aimed at studying the effects of gas concentration on particle shrinkage would benefit from more analytical equipment to measure both the aerosol and the ambient gas composition. Chemical analysis of the aerosol with an instrument like a High Resolution Time-of-Flight Aerosol Mass Spectrometer (HR-ToF-AMS) would provide some insight into the chemical constituents of the aerosol. While there was a HR-ToF-AMS onsite during the reported measurement period, analysis of the aerosol mass fractions was not performed. Controlled chamber experiments attempting to mimic this aerosol by varying concentrations of BVOCs and oxidants could also inform models seeking to predict aerosol growth rate. Field experiments in different locations would be beneficial as well. These experiments were performed in a location that was chosen specifically because it is affected by air masses coming from both an urban environment and from a surrounding forest. Environments more directly impacted by urban emissions should be studied, as well as rural environments that have different types of native plants that could produce vastly different BVOC mixtures and concentrations.

Based on the presented results, the species contributing to particle growth for several of the observed days may have become chemically changed after condensation, rendering them less volatile and contributing to a more stable aerosol population. It is also possible that the oxidized species formed were semi-volatile to begin with. Xu *et al*. (2015) theorized that the oxidation byproducts of nitrate radical and monoterpenes were responsible for a significant portion of the nighttime SOA growth. The presented data might have shown a correlation between high concentrations of nitrate radical and

monoterpenes with particle evaporation events (August 2 and 3), but more experiment days are necessary to show a definitive trend. Without knowing exactly what oxidants and oxidizable gases were contributing to particle growth, it is difficult to predict what combinations would lead to lower volatility products. No particular pattern in the measured gas concentrations was discerned that could fully explain either the magnitude of the growth rate or whether or not the growth rate would reverse with atmospheric perturbations. More data are needed to make more definite conclusions about what species led to particle growth, and what reactions (if any) took place to make them less volatile, but the presented data suggests that models that assume that the condensed species stay in equilibrium may be underestimating aerosol mass loading.

REFERENCES

ATKINSON, R. W., FULLER, G. W., ANDERSON, H. R., HARRISON, R. M. & ARMSTRONG, B. 2010. Urban Ambient Particle Metrics and Health: A Time-series Analysis. *Epidemiology,* 21**,** 501-511.

ATKINSON, R. W., KANG, S., ANDERSON, H. R., MILLS, I. C. & WALTON, H. A. 2014. Epidemiological time series studies of $PM_{2.5}$ and daily mortality and hospital admissions: a systematic review and meta-analysis. *Thorax*.

BENNETT, D. H., MARGNI, M. D., MCKONE, T. E. & JOLLIET, O. 2002. Intake Fraction for Multimedia Pollutants: A Tool for Life Cycle Analysis and Comparative Risk Assessment. *Risk Analysis,* 22**,** 905-918.

BENNETT, W. D. 2002. Rapid translocation of nanoparticles from the lung to the bloodstream? *American Journal of Respiratory and Critical Care Medicine,* 165**,** 1671-1672.

BOYD, C. M., NAH, T., XU, L., BERKEMEIER, T. & NG, N. L. 2017. Secondary Organic Aerosol (SOA) from Nitrate Radical Oxidation of Monoterpenes: Effects of Temperature, Dilution, and Humidity on Aerosol Formation, Mixing, and Evaporation. *Environmental Science & Technology,* 51**,** 7831-7841.

BUDISULISTIORINI, S. H., BAUMANN, K., EDGERTON, E. S., BAIRAI, S. T., MUELLER, S., SHAW, S. L., KNIPPING, E. M., GOLD, A. & SURRATT, J. D. 2016. Seasonal characterization of submicron aerosol chemical composition and organic aerosol sources in the southeastern United States: Atlanta, Georgia, and Look Rock, Tennessee. *Atmospheric Chemistry and Physics,* 16**,** 5171-5189.

CHUNG, S. H. & SEINFELD, J. H. 2002. Global distribution and climate forcing of carbonaceous aerosols. *Journal of Geophysical Research: Atmospheres,* 107**,** AAC 14-1-AAC 14-33.

CUSACK, M., ALASTUEY, A. & QUEROL, X. 2013. Case studies of new particle formation and evaporation processes in the western Mediterranean regional background. *Atmospheric Environment,* 81**,** 651-659.

DE GOUW, J. A., BROCK, C. A., ATLAS, E. L., BATES, T. S., FEHSENFELD, F. C., GOLDAN, P. D., HOLLOWAY, J. S., KUSTER, W. C., LERNER, B. M., MATTHEW, B. M., MIDDLEBROOK, A. M., ONASCH, T. B., PELTIER, R. E., QUINN, P. K., SENFF, C. J., STOHL, A., SULLIVAN, A. P., TRAINER, M., WARNEKE, C., WEBER, R. J. & WILLIAMS, E. J. 2008. Sources of particulate matter in the

northeastern United States in summer: 1. Direct emissions and secondary formation of organic matter in urban plumes. *Journal of Geophysical Research: Atmospheres,* 113**.**

DERWENT, R. G., COLLINS, W. J., JENKIN, M. E., JOHNSON, C. E. & STEVENSON, D. S. 2003. The Global Distribution of Secondary Particulate Matter in a 3-D Lagrangian Chemistry Transport Model. *Journal of Atmospheric Chemistry,* 44**,** 57-95.

FUENTES, J. D., GU, L., LERDAU, M., ATKINSON, R., BALDOCCHI, D., BOTTENHEIM, J. W., CICCIOLI, P., LAMB, B., GERON, C., GUENTHER, A., SHARKEY, T. D. & STOCKWELL, W. 2000. Biogenic Hydrocarbons in the Atmospheric Boundary Layer: A Review. *Bulletin of the American Meteorological Society,* 81**,** 1537-1575.

GRIESHOP, A. P., DONAHUE, N. M. & ROBINSON, A. L. 2007. Is the gas-particle partitioning in alpha-pinene secondary organic aerosol reversible? *Geophysical Research Letters,* 34.

GRIFFIN, R. J., COCKER, D. R., SEINFELD, J. H. & DABDUB, D. 1999. Estimate of global atmospheric organic aerosol from oxidation of biogenic hydrocarbons. *Geophysical Research Letters,* 26**,** 2721-2724.

GROSJEAN, D. & SEINFELD, J. H. 1989. Parameterization of the formation potential of secondary organic aerosols. *Atmospheric Environment (1967),* 23**,** 1733-1747.

HARRISON, R. M. & YIN, J. 2000. Particulate matter in the atmosphere: which particle properties are important for its effects on health? *Science of The Total Environment,* 249**,** 85-101.

HENZE, D. K. & SEINFELD, J. H. 2006. Global secondary organic aerosol from isoprene oxidation. *Geophysical Research Letters,* 33.

IPCC 2013. *Climate Change 2013: The Physical Science Basis. Contribution of Working Group I to the Fifth Assessment Report of the Intergovernmental Panel on Climate Change,* Cambridge, United Kingdom and New York, NY, USA, Cambridge University Press.

JIMENEZ, J. L., CANAGARATNA, M. R., DONAHUE, N. M., PREVOT, A. S. H., ZHANG, Q., KROLL, J. H., DECARLO, P. F., ALLAN, J. D., COE, H., NG, N. L., AIKEN, A. C., DOCHERTY, K. S., ULBRICH, I. M., GRIESHOP, A. P., ROBINSON, A. L., DUPLISSY, J., SMITH, J. D., WILSON, K. R., LANZ, V. A., HUEGLIN, C., SUN, Y. L., TIAN, J., LAAKSONEN, A., RAATIKAINEN, T., RAUTIAINEN, J.,

VAATTOVAARA, P., EHN, M., KULMALA, M., TOMLINSON, J. M., COLLINS, D. R., CUBISON, M. J., DUNLEA, J., HUFFMAN, J. A., ONASCH, T. B., ALFARRA, M. R., WILLIAMS, P. I., BOWER, K., KONDO, Y., SCHNEIDER, J., DREWNICK, F., BORRMANN, S., WEIMER, S., DEMERJIAN, K., SALCEDO, D., COTTRELL, L., GRIFFIN, R., TAKAMI, A., MIYOSHI, T., HATAKEYAMA, S., SHIMONO, A., SUN, J. Y., ZHANG, Y. M., DZEPINA, K., KIMMEL, J. R., SUEPER, D., JAYNE, J. T., HERNDON, S. C., TRIMBORN, A. M., WILLIAMS, L. R., WOOD, E. C., MIDDLEBROOK, A. M., KOLB, C. E., BALTENSPERGER, U. & WORSNOP, D. R. 2009. Evolution of Organic Aerosols in the Atmosphere. *Science,* 326**,** 1525-1529.

NATIONAL OCEANIC AND ATMOSPHERIC ASSOCIATION, AIR RESOURCES LABORATORY. NOAA Hysplit Trajectory Model. Web. https://ready.arl.noaa.gov/hypub-bin/trajtype.pl

NG, N. L., CHHABRA, P. S., CHAN, A. W. H., SURRATT, J. D., KROLL, J. H., KWAN, A. J., MCCABE, D. C., WENNBERG, P. O., SOROOSHIAN, A., MURPHY, S. M., DALLESKA, N. F., FLAGAN, R. C. & SEINFELD, J. H. 2007. Effect of NO_x level on secondary organic aerosol (SOA) formation from the photooxidation of terpenes. *Atmos. Chem. Phys.,* 7**,** 5159-5174.

PANDIS, S. N., WEXLER, A. S. & SEINFELD, J. H. 1993. Secondary organic aerosol formation and transport — II. Predicting the ambient secondary organic aerosol size distribution. *Atmospheric Environment. Part A. General Topics,* 27**,** 2403-2416.

ROLLINS, A. W., BROWNE, E. C., MIN, K.-E., PUSEDE, S. E., WOOLDRIDGE, P. J., GENTNER, D. R., GOLDSTEIN, A. H., LIU, S., DAY, D. A., RUSSELL, L. M. & COHEN, R. C. 2012. Evidence for NO_x Control over Nighttime SOA Formation. *Science,* 337**,** 1210-1212.

ROLLINS, A. W., KIENDLER-SCHARR, A., FRY, J. L., BRAUERS, T., BROWN, S. S., DORN, H. P., DUBÉ, W. P., FUCHS, H., MENSAH, A., MENTEL, T. F., ROHRER, F., TILLMANN, R., WEGENER, R., WOOLDRIDGE, P. J. & COHEN, R. C. 2009. Isoprene oxidation by nitrate radical: alkyl nitrate and secondary organic aerosol yields. *Atmos. Chem. Phys.,* 9**,** 6685-6703.

SANDER, S., FRIEDL, R., GOLDEN, D., KURYLO, M., HUIE, R., ORKIN, V., MOORTGAT, G., RAVISHANKARA, A. R., E. KOLB, C., MOLINA, M. & FINLAYSON-PITTS, B. 2003. Chemical Kinetics and Photochemical Data for Use in Atmosheric Studies; JPL Publication 02-25.

SEINFELD, J. & PANDIS, S. 2016. Atmospheric Chemistry and Physics: From Air Pollution to Climate Change. *John Wiley & Sons, Inc.* Hoboken, New Jersey

SKRABALOVA, L., ZIKOVA, N. & ZDIMAL, V. 2015. Shrinkage of Newly Formed Particles in an Urban Environment. *Aerosol and Air Quality Research,* 15**,** 1313-1324.

TANI, A., HAYWARD, S. & HEWITT, C. N. 2003. Measurement of monoterpenes and related compounds by proton transfer reaction-mass spectrometry (PTR-MS). *International Journal of Mass Spectrometry,* 223**,** 561-578.

TEXAS COMMISSION ON ENVIRONMENTAL QUALITY. UH WG Jones Forest C698 Data by Site by Date (all parameters), 06 October 2017. Web. 08 Nov 17. https://www.tceq.texas.gov/cgi-bin/compliance/monops/daily_summary.pl

TSIGARIDIS, K. & KANAKIDOU, M. 2003. Global modelling of secondary organic aerosol in the troposphere: a sensitivity analysis. *Atmos. Chem. Phys.,* 3**,** 1849-1869.

WIKOL, M., HARTMANN, B., BRENDLE, J., CRANE, M., BEUSCHER, U., BRAKE, J. & SHICKEL, T. 2007. Expanded Polytetrafluoroethylene Membranes and Their Applications. *Filtration and Purification in the Biopharmaceutical Industry, Second Edition.* CRC Press.

XU, L., GUO, H., BOYD, C. M., KLEIN, M., BOUGIATIOTI, A., CERULLY, K. M., HITE, J. R., ISAACMAN-VANWERTZ, G., KREISBERG, N. M., KNOTE, C., OLSON, K., KOSS, A., GOLDSTEIN, A. H., HERING, S. V., DE GOUW, J., BAUMANN, K., LEE, S.-H., NENES, A., WEBER, R. J. & NG, N. L. 2015. Effects of anthropogenic emissions on aerosol formation from isoprene and monoterpenes in the southeastern United States. *Proceedings of the National Academy of Sciences,* 112**,** 37-42.

YOUNG, L. H., LEE, S.-H., KANAWADE, V., HSIAO, T.-C., L. LEE, Y., HWANG, B.-F., LIOU, Y. J., HSU, H.-T. & TSAI, P.-J. 2012. *New particle growth and shrinkage observed in subtropical environments*.

ZHANG, Q., JIMENEZ, J. L., CANAGARATNA, M. R., ALLAN, J. D., COE, H., ULBRICH, I., ALFARRA, M. R., TAKAMI, A., MIDDLEBROOK, A. M., SUN, Y. L., DZEPINA, K., DUNLEA, E., DOCHERTY, K., DECARLO, P. F., SALCEDO, D., ONASCH, T., JAYNE, J. T., MIYOSHI, T., SHIMONO, A., HATAKEYAMA, S., TAKEGAWA, N., KONDO, Y., SCHNEIDER, J., DREWNICK, F., BORRMANN, S., WEIMER, S., DEMERJIAN, K., WILLIAMS, P., BOWER, K., BAHREINI, R., COTTRELL, L., GRIFFIN, R. J., RAUTIAINEN, J., SUN, J. Y., ZHANG, Y. M. & WORSNOP, D. R. 2007. Ubiquity and dominance of oxygenated species in organic aerosols in anthropogenically-influenced Northern Hemisphere midlatitudes. *Geophysical Research Letters,* 34.